LITHOS 482–483 (2024) 107695

Contents lists available at ScienceDirect

LITHOS

journal homepage: www.elsevier.com/locate/lithos

Understanding the links between volcanic systems and epithermal ore formation: A case study from Conical Seamount, Papua New Guinea

Louis-Maxime Gautreau [a,*], Thor H. Hansteen [a], Maxim Portnyagin [a], Christoph Beier [b], Matthias Frische [a], Philipp A. Brandl [a]

[a] GEOMAR Helmholtz Centre for Ocean Research Kiel, Wischhofstraße 1-3, 24148 Kiel, Germany
[b] Research Programme of Geology and Geophysics (GeoHel), Department of Geosciences and Geography, PO Box 64, FIN-00014, University of Helsinki, Finland

ARTICLE INFO

Keywords:
Conical Seamount
Magma chamber
Melt inclusions
Magmatic sulfides
Fluid

ABSTRACT

The Tabar-Lihir-Tanga-Feni (TLTF) island chain in northeastern Papua New Guinea formed by tectonic and alkaline to shoshonitic magmatic activity since the Pliocene. Several volcanic centers are Cu—Au mineralized including the world-class Ladolam Au deposit and Conical Seamount south of Lihir. The latter has been recognized as a juvenile analogue to the Ladolam deposit located on-shore. Whereas the mineralization at Conical Seamount is reasonably well studied, the specific magmatic processes that promote epithermal mineralization at this seamount but not at others are poorly understood. Here, we present new petrological and geochemical data from Conical Seamount, and compare them with those from the barren (unmineralized) Edison, Tubaf and New World seamounts nearby. We focus on whole rock compositions and major and trace element analysis of melt inclusions and minerals including clinopyroxene, sulfide and magnetite. We combine our observations with modelled constraints on mantle source composition and partial melting as well as magma evolution. A first-stage melting leaves a residual mantle source enriched in Au. Second-stage melting of a previously subduction-metasomatized mantle generally promotes the transfer and concentration of metals and volatiles in the ascending melts. These magmas are unlikely to control ore formation as all seamounts show evidence for similar mantle sources and parental melt composition. However, the presence of a shallow crustal magma chamber is unique to Conical Seamount. It is characterized by frequent melt replenishments and extensive magma fractionation leading to sulfide and magmatic volatile saturation. These specific magma chamber processes lead to the pre-enrichment of the magma in chalcophile elements including Au, while sulfide saturation coeval with magmatic volatile exsolution provide the way for an effective Au transfer from the magmatic to the epithermal system.

1. Introduction

Papua New Guinea (PNG) in the western Pacific is known for spectacular endowment in Cu- and Au-rich mineral systems that are intimately related to its vital and young plate tectonic evolution. Episodic subduction and collisional tectonics led to widespread magmatism since the Eocene and ultimately to the formation of some of the world's largest and youngest porphyry Cu deposits. Most of these porphyry Cu systems in PNG are associated with calc-alkaline magmatic suites of Miocene age (e.g., Hammarstrom et al., 2013; Holm et al., 2019). More recent microplate tectonics, involving slab stagnation and tearing following collision combined with extensional settings, control post-subduction alkaline magmatism, which led to the formation of Au-rich mineral deposits since the Pliocene (Holm et al., 2019; Richards, 2009).

More than half of the tonnage of total contained Au in the most recently formed deposits occurs in the Tabar-Lihir-Tanga-Feni (TLTF) island chain in north-eastern PNG (Fig. 1). The island chain is characterized by high-K alkaline and shoshonitic volcanism and is host to the Ladolam mine on Lihir, the world's largest alkaline epithermal gold deposit (Cooke et al., 2020). One other deposit (Simberi) is actively exploited, but at least six further prospects indicate the region's high Au potential (Brandl et al., 2020). It is important to note that Au exploration is not restricted to the onshore. There are several submarine exploration tenements in the area, one of which is located at Conical Seamount, a

* Corresponding author.
E-mail addresses: lgautreau@geomar.de (L.-M. Gautreau), thansteen@geomar.de (T.H. Hansteen), mportnyagin@geomar.de (M. Portnyagin), christoph.beier@helsinki.fi (C. Beier), mfrische@geomar.de (M. Frische), pbrandl@geomar.de (P.A. Brandl).

https://doi.org/10.1016/j.lithos.2024.107695
Received 15 December 2023; Received in revised form 17 May 2024; Accepted 5 June 2024
Available online 22 June 2024
0024-4937/© 2024 Published by Elsevier B.V.

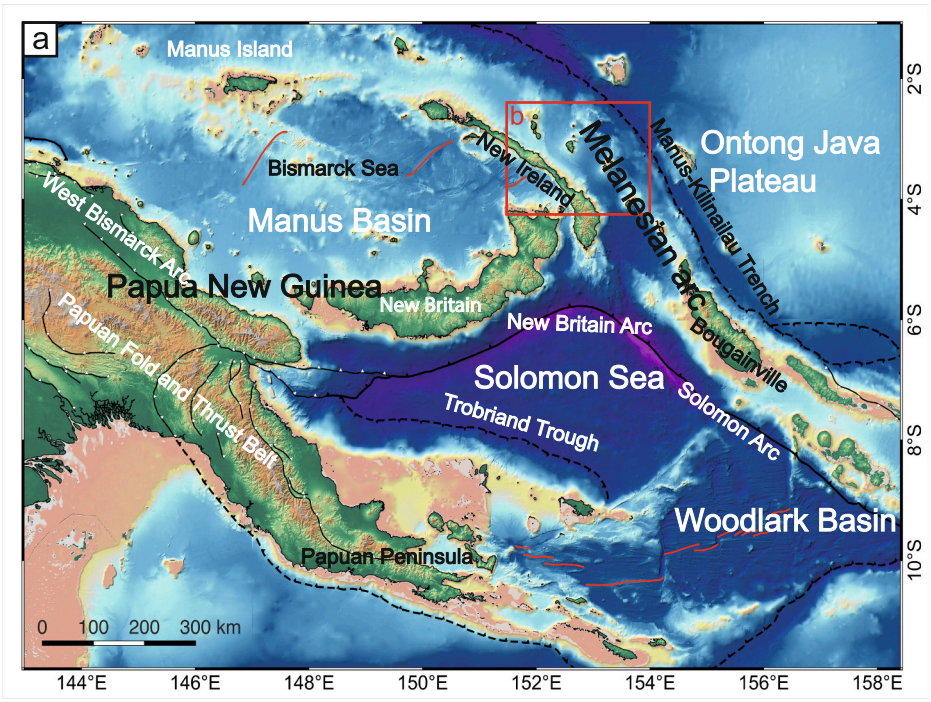

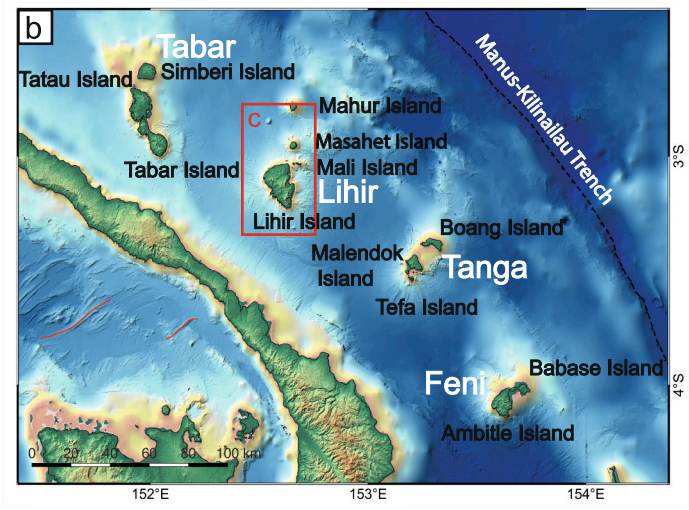

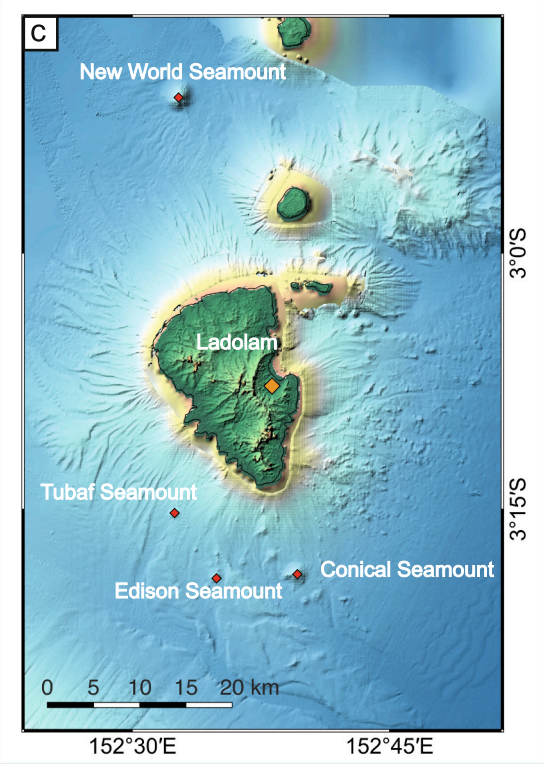

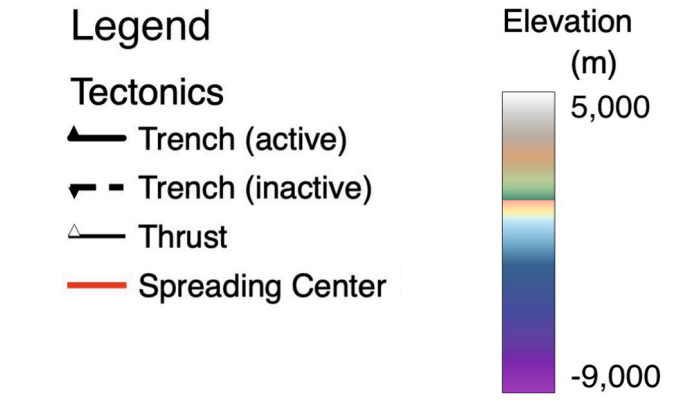

Fig. 1. Regional settings of Conical Seamount a: Map of the eastern Papua New Guinean Archipelago with main structural features. b: Map of the TLTF island chain with the name of the four island groups in white and the individual main islands in black. c: Location of the different seamounts (red diamonds) surrounding Lihir island. The location of the Ladolam Au deposit on Lihir island is marked by the orange diamond. (For interpretation of the references to colour in this figure legend, the reader is referred to the web version of this article.)

submarine volcano south of Lihir island. This is also the site where an epithermal-style mineralization was first discovered at the seafloor (Petersen et al., 2002). Additionally, Conical Seamount has been interpreted as a potential juvenile analogue to the Luise volcano hosting the world-class Ladolam Au deposit on Lihir (Müller et al., 2003).

Conical Seamount is only one of several seamounts around Lihir. Many of these seamounts are clustered in a volcanic field south of Lihir, only New World Seamount is located northwest of Lihir (Fig. 1). These seamounts have been in the center of scientific attention due to the abundant mantle and crustal xenolith cargo at Tubaf Seamount (Bénard et al., 2021; Franz and Romer, 2010; McInnes et al., 2001; Renno et al., 2004; Soustelle et al., 2013) and the Au-rich mineralization at Conical Seamount (Müller et al., 2003; Petersen et al., 2002). However, less attention was given to why Conical Seamount is the sole mineralized seamount in an area that otherwise has proven to be prolific for magmatic-hydrothermal Cu—Au mineralization.

The present study provides detailed petrological-geochemical insights of Conical Seamount in order to decipher its magma plumbing system and its distinctive characteristics in comparison to the other volcanic centers in the region. We focus on petrographic observations and mineral chemistry of the host lavas. Additionally, we present major and trace element analyses of melt inclusions and whole-rock samples. We use this geochemical data together with modelling results to study the different stages of magma genesis under the Conical Seamount beginning from partial melting of the subduction-modified mantle to magma evolution in the shallow crustal reservoir that may be unique among the seamounts in the area. Finally, we discuss our findings in the context of magmatic-hydrothermal ore formation at this seamount as well as epithermal mineral potentials in general.

2. Geological setting

The TLTF island chain is located in north-eastern Papua New Guinea, along the complex collision zone between the Pacific and the Australian Plate. The subduction of the Pacific Plate beneath the Australian Plate started during the Eocene (at 43–42 Ma) and led to the formation of the Melanesian Arc. It encompasses the islands of New Britain, New Ireland and Bougainville in eastern Papua New Guinea, as well as the Solomon Islands and Vanuatu. It stopped in the late Oligocene at 25–20 Ma, when the Ontong Java Plateau (Mann and Taira, 2004; Taylor, 2006) docked into the subduction zone and caused a slab break-off at 20–15 Ma. Subduction reversed to a north-easterly direction in the late Miocene, forming the now active San Cristobal/South Solomon–New Britain trenches (e.g., Mann and Taira, 2004; Petterson et al., 1999).

Recent magmatic activity in Papua New Guinea is related to a complex interplay of rifting (Papuan Peninsula and offshore on the Trobriand Platform: e.g., Baldwin et al., 2012), seafloor spreading (Bismarck Sea Taylor, 1979), collision (Papuan Fold and Thrust Belt: e.g., Holm et al., 2015), and a transition from subduction to collision (West Bismarck Arc: e.g., Abbott, 1995; Woodhead et al., 2010) and active subduction (New Britain arc, Bougainville and the Solomon arc: e.g., Petterson et al., 1999; Schuth et al., 2009). The geochemistry of the lavas erupted along the Tabar-Lihir-Tanga-Feni (TLTF) island chain indicates a volcanic arc origin (Stracke and Hegner, 1998) even though the lavas are post-dating active subduction along the Manus-Kilinailau Trench. The TLTF lavas erupt behind the arc front of the current subduction at the New Britain Trench. The magmas ascended through up to 6 km of sediments in the New Ireland Basin (Exon & Marlow, 1988) that formed in a forearc setting along the Manus-Kilinailau Trench. Melting was triggered by incipient rifting in response to the collision with the Ontong Java Plateau and crustal fragmentation at the margin of the North Bismarck Microplate (Brandl et al., 2020).

The first islands of the TLTF volcanic chain formed in the Mid Pliocene (Simberi and Tatau from the Tabar island group: Wallace et al., 1983; McInnes, 1992; Rytuba et al., 1993) with the main phase of volcanic activity in the Pleistocene (Lihir, Tanga and Feni island groups: Wallace et al., 1983; Davies and Ballantyne, 1987; Moyle et al., 1990; Rytuba et al., 1993; Renno et al., 2004). Holocene activity is known from Ambitle in the Feni island group (Horz et al., 2004; Licence et al., 1987). With an overall age of <4 Ma, the TLTF volcanism is very young compared to other parts of Papua New Guinea (Brandl et al., 2020).

Volcanic rocks of the TLTF island chain are highly alkaline and mostly shoshonitic (Brandl et al., 2020). Whereas the islands show a wide compositional range from trachybasalt to highly evolved (quartz-) trachyte, the submarine volcanoes erupted exclusively trachybasalt or basaltic trachyandesite (Brandl et al., 2020; Stracke and Hegner, 1998). The more mafic and more restricted compositional range of rocks erupted at the seafloor led to the conclusion that these seamounts may represent potential juvenile analogues to the large composite volcanoes onshore (Stracke and Hegner, 1998). Each of the four largest seamounts New World, Tubaf, Edison and Conical Seamount (Fig. 1c) shows its own characteristics: New World Seamount in the NW erupted the most evolved compositions of the seamounts (basaltic trachyandesites: e.g. Stracke and Hegner, 1998). Tubaf Seamount is well known for the large amount of crustal and mantle xenoliths entrained in the erupted volcanics (e.g. McInnes et al., 2001). Edison Seamount hosts two active, low-temperature hydrothermal fields (Herzig et al., 1994). Conical Seamount, the largest of the volcanic edifices with 600 m elevation above the surrounding seafloor (summit at 1050 m below sea level), is host to Au-rich epithermal-style mineralization (Müller et al., 2003; Petersen et al., 2002). Despite their close spatial proximity, previous research suggested distinct magma plumbing systems at these seamounts (Kamenov et al., 2005). Magmas at Edison and Tubaf seamounts ascended rapidly from the upper mantle and lower crustal depths (Kamenov et al., 2005). In contrast, a shallow crustal magma reservoir likely exists underneath Conical Seamount (Kamenov et al., 2005). It has been proposed to be important for magmatic-hydrothermal ore-forming processes and is thus the focus of our study.

3. Methods

3.1. Sample recovery and bulk rock analyses

Several cruises with the German research vessel R/V SONNE targeted and sampled the area: SO-94 in 1994, SO-133 in 1998 and SO-166 in 2002 (Herzig, 2002; Herzig et al., 1994; Herzig et al., 1998). The samples used for this study were all recovered during these expeditions as well as during the Australian SHAARC (Investigation of Submarine, Hydrothermally Active ARC Volcanoes in the Tabar-Lihir-Tanga-Feni Island and Solomon Island Chains) cruise of the R/V Franklin (04/00) in 2000 (Mcinnes et al., 2000).

Fresh lava samples from Conical, Edison, Tubaf and New World seamounts suitable for geochemical analyses were selected visually. SHAARC samples, along with samples from the study by Stracke and Hegner (1998) for which the complete set of trace elements has not been acquired previously, were analyzed at the GeoZentrum Nordbayern (GZN; FAU Erlangen-Nürnberg) using X-ray fluorescence and Inductively Coupled Plasma Mass Spectrometry (ICPMS) (detailed instrumentation in supplementary information). A representative subset of whole rock samples was selected for high precision trace element analyses (including Ag, As, Au, Sb) using nanopowder pressed tablets and Laser Ablation (LA-) ICPMS at the Institute of Geosciences of the University of Kiel. The bulk samples with a loss on ignition higher than 1.5 wt% are likely to be slightly altered and were thus excluded from the dataset used in this study. The results presented here are all volatile-free and normalized to 100 wt% sum of oxides.

3.2. Petrography and mineral and melt inclusion chemistry

The mineral chemistry of 24 representative rock samples from Conical Seamount (sampled during SO-94, SO-133 and SO-166) and, for comparison, one sample each from Edison, Tubaf and New World

seamounts were described and discussed.

Major and minor elements in minerals, melt inclusions and groundmass glasses were analyzed using a JEOL JXA 8200 electron microprobe at the GEOMAR Helmholtz Centre for Ocean Research Kiel (Germany). The analytical conditions are described in detail in the supplementary methods section. Compositional profiles of pyroxene phenocrysts were determined in samples 68DR-1 A and —1C from Conical Seamount. Groundmass glass was analyzed from three samples (68DR1-C, 50DR1B and 7DR2E). Trace elements and selected major elements of representative sulfides, matrix glass, melt inclusions and clinopyroxene crystals were determined using LA-ICP-MS at GEOMAR (detailed instrument description in supplementary information).

3.3. Melt inclusion analysis and post-entrapment correction

The melt inclusions in clinopyroxene phenocrysts were glassy or partly crystallized, and occasionally contained visible crystals that were likely formed after melt entrapment. We aimed at analyzing only glassy inclusions. Some analytical results were apparently still compromised by entrapped mineral phases as identified by their exotic composition, and were thus excluded from further discussion (details about the filtering process are described in the supplementary information). Here, we discuss the composition of 287 melt inclusions from Conical Seamount, five inclusions from Edison Seamount and three inclusions from Tubaf Seamount. Judging from their low Mg#, most melt inclusions were subject to post-entrapment crystallization on the inclusion walls (e.g., Rose-Koga et al., 2021). In order to estimate the initial compositions of the melt inclusions, we modelled adding the host clinopyroxene composition to the melt inclusion composition until equilibrium with the host clinopyroxene was reached. The equilibrium Fe—Mg partitioning was estimated using the model of Duke (1976), which agrees well with more recent models (e.g., Klügel and Klein, 2006; Putirka, 2008).

Full details of all the methods used for this study and the results can be found in the supplements.

4. Results

4.1. Petrography and mineral chemistry

4.1.1. Major petrographic features

Petrographic and petrologic observations of lavas from the various seamounts around Lihir yielded significant differences, in agreement with previous studies (Kamenov et al., 2005; McInnes et al., 2001; Müller et al., 2003). The main phenocryst phases in the trachybasalts from Conical Seamount are euhedral clinopyroxene (up to 6 mm, average 20–25 area %), plagioclase (up to 1 mm, 5–10 area %) and magnetite (20 μm to 200 μm, up to 3 area %) in a fine-grained groundmass composed of clinopyroxene, plagioclase, magnetite and accessory apatite microlites in residual glass (Fig. 2a). The plagioclase crystals have an anorthite component ranging from An_{73} to An_{95}. Olivine and very rare amphibole and phlogopite phenocrysts also occur. In addition, we observed 10–50 μm magmatic sulfides in the groundmass (Fig. 2c), not described in previous studies. The rock samples display a variable vesicularity from 1% to 15 area %.

At Conical Seamount, glomerophyric intergrowths of clinopyroxene and other minerals are common in all samples, and can be assigned to different types. A common variety consists of two or three crossing clinopyroxene crystals (Fig. 3b). Larger crystals (up to above 5 mm) may occur as stellar-like structures, where three to six clinopyroxene crystals protrude in several directions from a central core consisting of one or several smaller, irregular clinopyroxene crystals (Fig. 3a). Magnetite can occur within these structures, between the outer clinopyroxene grains or in the glomerocryst core. Another common variety is a mixture of the main phenocryst phases clinopyroxene, plagioclase and magnetite (Fig. 3d), although clinopyroxene remains the dominant phase.

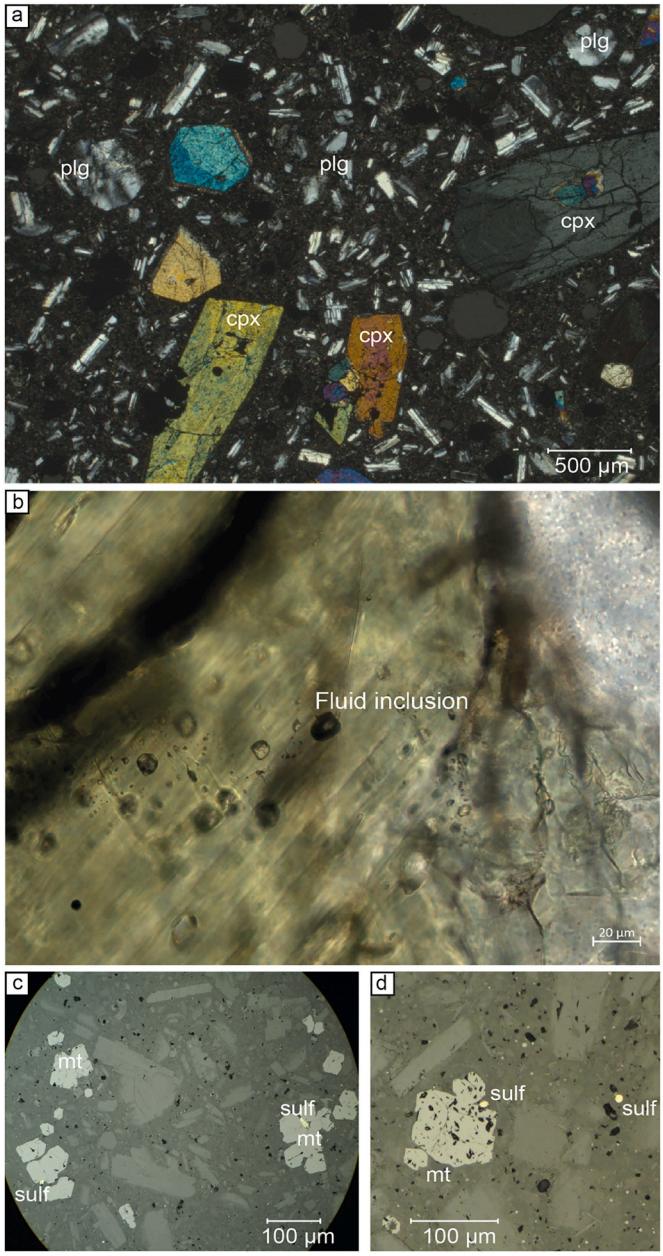

Fig. 2. Petrographic features of samples from Conical Seamount. a) Clinopyroxene (cpx) and plagioclase (plg) phenocrysts in fine-grained groundmass (sample 27RD10–20, optical image, transmitted, cross-polarized light). b) Primary fluid inclusions (FI) in clinopyroxene phenocryst (sample 39RD30–40, optical image, transmitted, plain polarized light); c) and d) Magnetite (mt) and sulfides (sulf) in groundmass (c – sample 14RD20–30, d – sample 37RD0–20; optical image, reflected light).

The clinopyroxene phenocrysts in Conical Seamount rocks commonly contain abundant melt inclusions, and to a lesser extent, fluid inclusions (Fig. 2b). The fluid inclusions occur isolated or in trails parallel to the growth zones of the host crystal (Fig. 2b). Secondary fluid inclusions crossing zones within a crystal are also common.

The trachybasalts from Edison and Tubaf seamounts contain elongated phenocrysts of phlogopite (up to 1.4 mm, 2 area %), amphibole (0.3 mm, 13 area %) and, to a lesser extent of clinopyroxene (up to 1 mm, 2 area %). Their fine-grained groundmass contains microlites of amphibole, clinopyroxene, plagioclase and magnetite in volcanic glass.

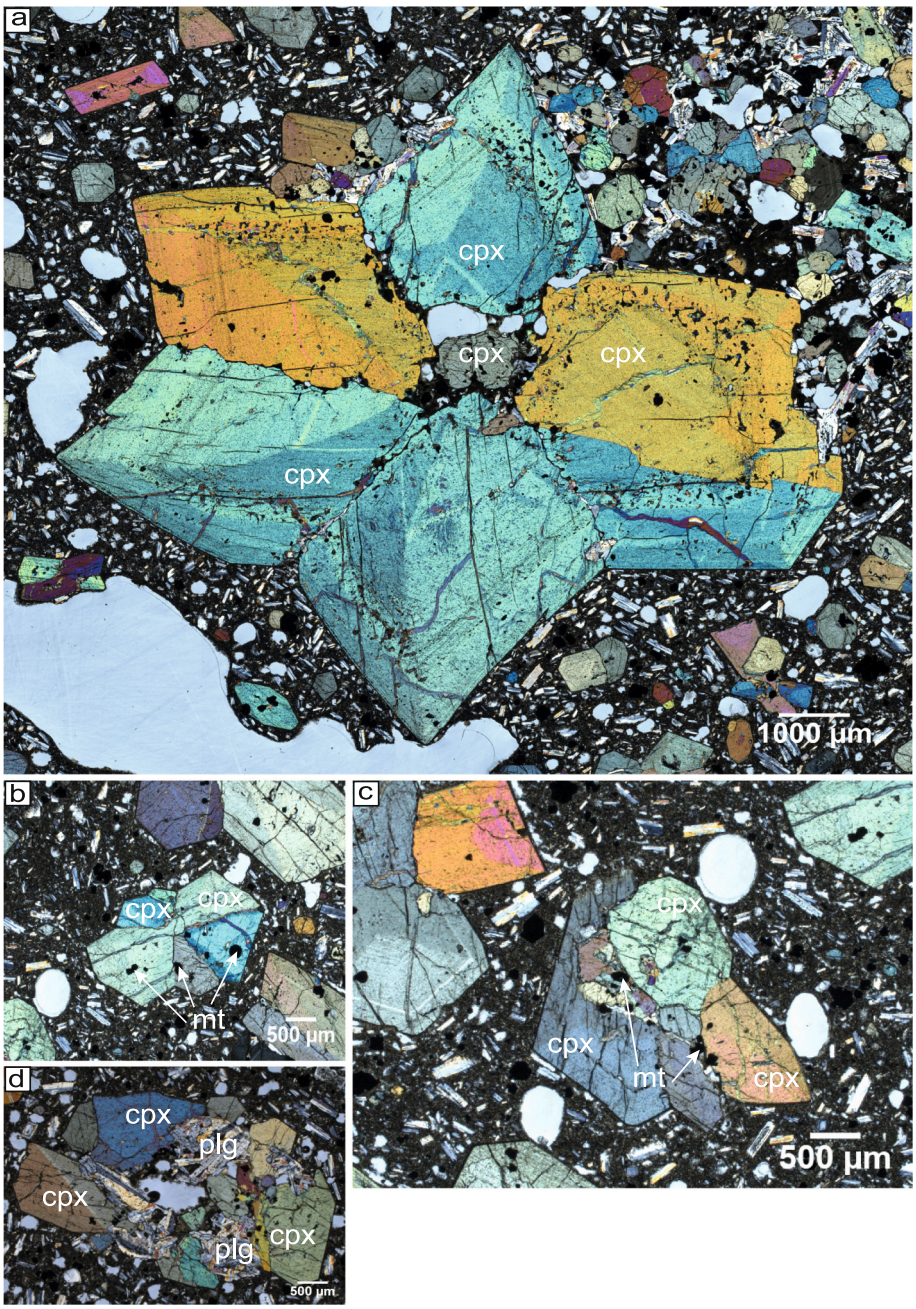

Fig. 3. Microscopic pictures of glomerophyric intergrowths at Conical Seamount (cross-polarized light). a) Stellar-like glomerophyric intergrowth with sector zonations (Sample 42RD10—22a). b) Orthogonal growth of different clinopyroxene and plagioclase crystals creating glomerophyric intergrowths (Sample 39RD30–40). c) Glomerophyric intergrowths (Sample 39RD30–40). d) Glomerophyric intergrowths resulting from crystal accumulation (Sample 48RD25–40).

4.1.2. Peculiarities of clinopyroxene phenocrysts

The clinopyroxene crystals at Conical Seamount are unusually large and range from ~100 µm to several millimeters, and often occur as the dominant phase in glomerocrystic intergrowths. The clinopyroxene crystals are commonly optically and chemically zoned. This zonation can be oscillatory, reverse, core-normal and sector-divided (Fig. 4). The transition between different zones is typically compositionally abrupt (Fig. 4). The primitive, oscillatory and core zonations have a large Mg# range (between 75 and 90 mol%). The high Mg# in these growth zones (Fig. 4) is usually associated with higher Cr_2O_3 contents of up to 0.45 wt %, low Al^{IV} (Al in tetrahedral configuration in the clinopyroxene formula unit, below 0.17 and down to 0.06) and low Tschermak component (sum of CrCa-Ts, $CaCr_2SiO_6$, Ca-Ts, $CaAl_2SiO_6$, CaTi-Ts, $CaTiAl_2O_6$ and CaFe-Ts, $CaFeAlSiO_6$, below 0.16 and down to 0.06). The primitive oscillatory zonation layers ranges from 10 to almost 100 µm with an average width of ~50 µm. The less magnesian zones in between have a width of 100 µm to several hundreds of micrometers. These zones in the clinopyroxene crystals display lower and less variable Mg# (between 66 and 77 mol%, Fig. 4) and higher Ts-component (0.16–0.20, Fig. 4).

By comparison, clinopyroxene phenocrysts from Tubaf and Edison seamounts are commonly <700 µm and almost unzoned with only 10–30 µm-wide outer rims. The clinopyroxene Mg# ranges from 80 to 86 mol% at Edison Seamount and from 79 to 84 mol% at Tubaf Seamount. Their Al^{IV} and Tschermak component range respectively from 0.07 to 0.12 and from 0.06 to 0.11.

Thus, the high Mg# zones in the clinopyroxene crystals at Conical Seamount are similar to the clinopyroxene minerals at Tubaf and Edison Seamount with high Cr-content, low Tschermak component and Al^{IV}.

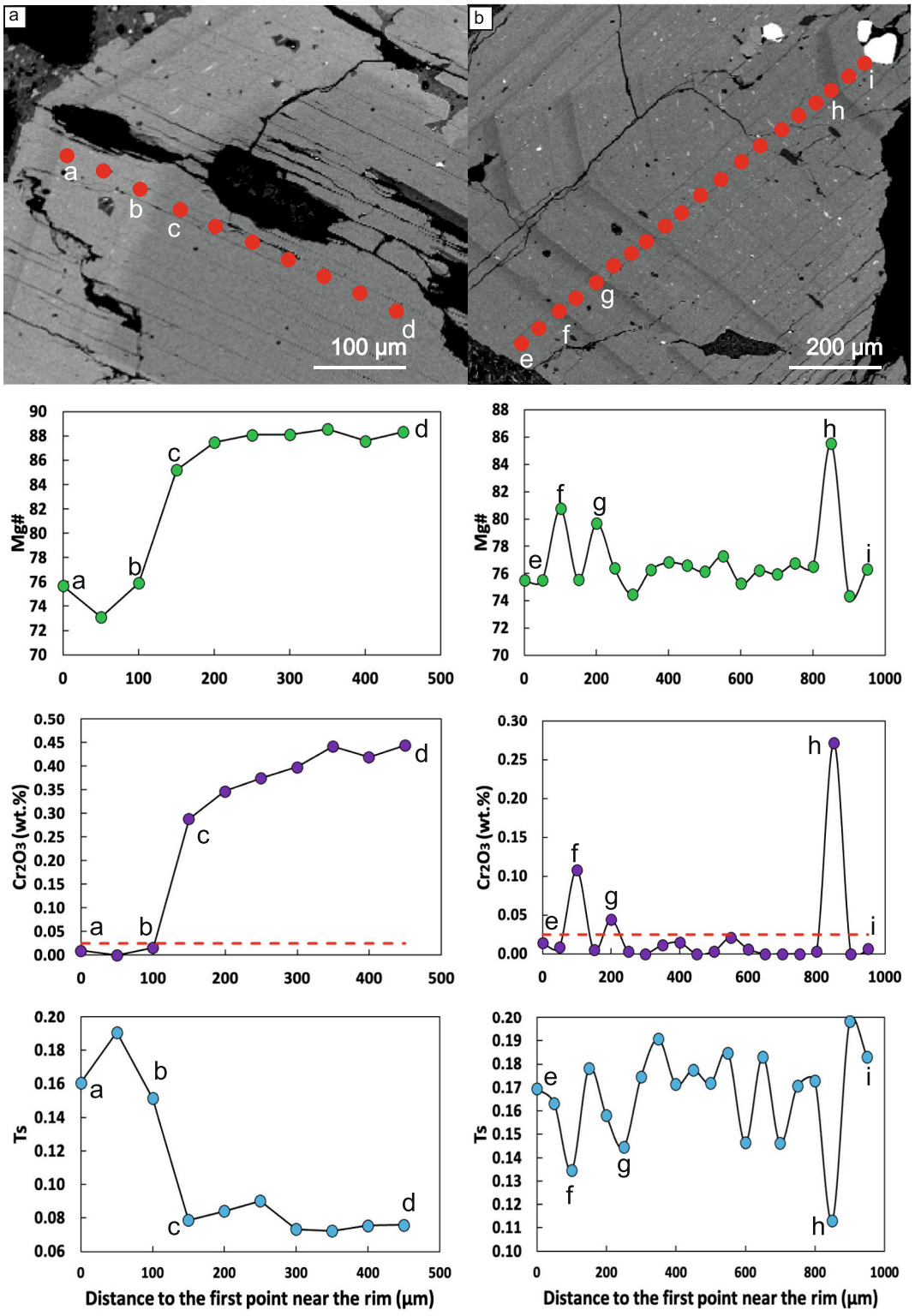

Fig. 4. Examples of chemical zoning in clinopyroxene crystals (backscattered electron image). A) Crystal from sample 68DR1A_2 showing a normal-core zonation and b) from sample 68DR1CB_8 showing oscillatory zonation. The detection limit for Cr_2O_3 measurements is shown by dashed red line. Primitive core antecrysts, as well as darker oscillatory zonations, are characterized by higher Mg#, high Cr_2O_3 and lower Tschermak (Ts) component. The oscillatory zonation bands have a sharp transition with the zones located towards the core and a more gradual transition with the zones located towards the rim. (For interpretation of the references to colour in this figure legend, the reader is referred to the web version of this article.)

However, the low Mg# zones in the clinopyroxene phenocrysts with low Cr-content, high Tschermak component and high Al^{IV} are specific to Conical Seamount.

4.1.3. *Sulfides*

Magmatic sulfides occur in almost all samples from Conical Seamount. These sulfides (sizes ranging from 10 to 50 µm, Fig. 2) are often associated with magnetite crystals. In such cases, sulfide crystals

may occur inside or between different aggregated magnetite crystals (Fig. 2c). The other type of sulfide occurs in rock groundmass and often displays a spherical droplet shape (size 10–20 μm, Fig. 2d). Magnetite-sulfide pairs can also occur as inclusions in clinopyroxene. Some sulfide phases have a lighter colour in reflected light and show some alteration features (irregular borders, alteration rims). Altered sulfides are also observed in samples from the other seamounts.

We distinguish three groups of sulfides using petrographic observations and the Cu-Fe-S ternary diagram (Fig. 5). The first and biggest group represents an intermediate solid solution (ISS) between cubanite and bornite compositions. These occur exclusively at Conical Seamount except for a single occurrence at New World Seamount. Their Fe contents range from 5.2 wt% to 45.3 wt% and their Cu contents from 15.5 wt% to 57.6 wt%. They are defined by a linearly decreasing trend of Cu with increasing Fe values. According to the classification of Georgatou & Chiaradia (2020), this first group corresponds to their type 3 magmatic sulfide group, which is common for high-K calc-alkaline to shoshonitic magmas. These magmatic sulfides have measured Au and Ag contents ranging from 0.6 to 45.7 μg/g and from 41.4 to 1397.2 μg/g respectively. The second group of sulfides is composed of pyrite and occurs solely at Conical Seamount. These pyrites have low Cu contents of <<5 wt% and Fe contents between 43.7 and 47.4 wt%. The third group comprises sulfides found in samples from New World and Edison seamounts. These sulfides have high Fe contents between 58.2 and 61.6 wt % with Cu contents of <3.1 wt% and thus corresponds to pyrrhotite solid solution. Due to their petrographic appearance and alteration, the two groups of pyrite and pyrrhotite solid solution are interpreted to be of hydrothermal origin.

4.2. Melt inclusions in clinopyroxene

We identify two major types of glassy melt inclusions occurring in clinopyroxene crystals at Conical Seamount (Fig. 6). Type 1 are primary inclusions, representing melt trapped during the crystallization of a crystal, and type 2 are pseudo-secondary or largely irregular inclusions occurring within sieve-textured clinopyroxene crystals, which presumably originated due to heating-induced resorption and later crystallization. We further divide type 1 into primary isolated melt inclusions (type 1a) and primary melt inclusions occurring in groups (type 1b). Type 1a melt inclusions have variable sizes from 10 μm to several hundred micrometers. Type 1b melt inclusions are smaller and range in size from 10 to 50 μm. Type 2 melt inclusions are divided into two subgroups:

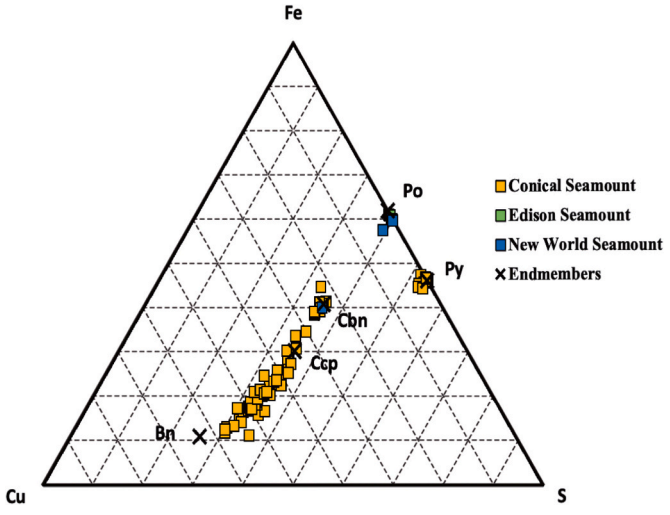

Fig. 5. Composition of the sulfide minerals from the Lihir seamounts within the Cu-Fe-S ternary diagram. Sulfide endmembers are displayed with black crosses (Bn = Bornite, Ccp = Chalcopyrite, Cbn = Cubanite, Py = Pyrite, Po = Pyrrhotite).

inclusions forming sieve texture inside pyroxene crystals (type 2a) and inclusions located in phenocryst cores and resulting from complete, or almost complete, resorption of the original clinopyroxene core, which we interpret to be of antecrystic origin (type 2b). Inclusions from both subgroups have variable sizes from 10 μm to several hundred micrometers. Besides melt inclusions enclosed inside pyroxenes, we observed common embayments of groundmass glass within phenocrysts and glass pockets between glomerocrysts.

The melt inclusions in the clinopyroxene crystals from Edison and Tubaf seamounts are classified as type 1. Pyroxenes with sieve textures are absent in rocks from these seamounts.

4.3. Rock and melt inclusion geochemistry

Whole-rocks from Conical Seamount record SiO_2 values ranging from 47.5 to 50.4 wt% and MgO values ranging from 4.5 to 6.7 wt%. With K_2O contents of about 3 wt% in the whole rocks, Conical Seamount lavas belong to the high-K rock series and classify as potassic trachybasalt (Le Maitre et al., 2002). Rocks from the other three sampled seamounts range from potassic trachybasalt to shoshonite.

The distinct types of melt inclusions at Conical Seamount described in the previous section exhibit substantial overlap in their chemical compositions (Figs. 7, 8). In contrast with the whole rocks, the compositions of melt inclusions in clinopyroxene are typically tephriphonolitic, and thus more evolved than whole rocks (Fig. 7). The SiO_2 contents of these melt inclusions range from 49.1 wt% to 57.1 wt%, with MgO values varying between 1.6 wt% and 5.0 wt% (see Figure). Melt inclusions from Edison (SiO_2 between 49.6 wt% and 51.9 wt% for MgO between 3.2 wt% and 4.7 wt%) and Tubaf (SiO_2 between 49.1 wt% and 52.1 wt% for MgO between 2.7 wt% and 3.8 wt%) seamounts exhibit similar compositional trends, typically representing phonotephrite compositions.

The groundmass glasses from Conical Seamount show much more restricted compositions and fall within the range of the melt inclusions (SiO_2 between 52.3 wt% and 53.6 wt% and MgO between 2.0 wt% and 2.6 wt%), confirming that the melts were evolved during crystallization and entrapment of the melt inclusions. Melt inclusions contain >5 wt% K_2O and thus confirm the shoshonitic nature of the magmas at Conical Seamount.

There is a general increase in Na, K and Al and a decrease in Fe and Ca with decreasing MgO (Fig. 8). Notably, TiO_2 and P_2O_5 cover a broad range of values, especially for low MgO, with an overall clustering between 0.4 and 0.6 wt% for both oxides.

The overall trend of decreasing FeO_t contents of the melt inclusions with decreasing MgO provides evidence for the crystallization of a Fe-rich phase, likely magnetite. However, the FeO_t content exhibits a notable scatter from 4.4 to 9.9 wt% FeO_t at a given MgO of ~5.0 to 3.2 wt%. Chlorine contents in the melt inclusions are relatively high and mostly range between 0.2 and 0.4 wt% with some outliers up to 0.6 wt%. Sulfur contents are 0.1 wt% and lower. Two inclusions from Tubaf Seamount have distinctively high S of 0.2–0.3 wt%.

The major and minor element compositions of melt inclusion from Conical, Edison and Tubaf seamounts overlap. However, the melt inclusions from Conical Seamount are predominantly more evolved in comparison with other seamounts (Fig. 8). Melt inclusions from Tubaf and Edison seamounts have distinctively high P_2O_5 contents of 0.8–1.6 wt%.

The Normal Mid-Ocean Ridge Basalt (N-MORB) normalized (Gale et al., 2013) trace element patterns of the bulk rocks from different seamounts are generally subparallel (Fig. 9a). They are characterized by an enrichment in the Large Ion Lithophile Elements (LILE: Cs, Rb, Ba, and Sr) and Pb, but also a depletion in High Field Strength Elements (HFSE: Nb, Ta, Zr, Hf and Ti) and to some extent heavy Rare Earth Elements (HREE: Dy, Ho, Er, Tm, Yb, Lu) compared to N-MORB.

Tubaf Seamount samples (MgO = 7.3–8.7 wt%) have lower LILE (Cs, Rb, Ba) but generally higher concentrations of the less incompatible

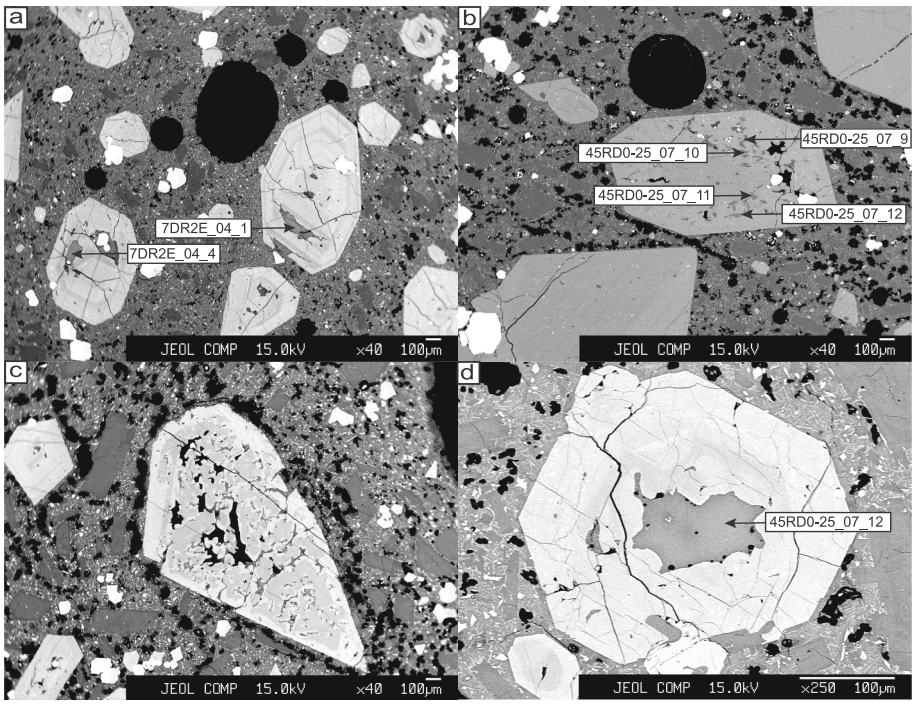

Fig. 6. Backscattered electron images of melt inclusions in pyroxene from Conical Seamount. a) Primary melt inclusions of type 1a in growth zones (Sample 7DR2E). b) Group of primary melt inclusions of type 1b in a growth zone (Sample 45RD0–25). c) Resorbed pyroxene with sieve texture comprising numerous melt and fluid inclusions of type 2a in clinopyroxene antecryst (Sample 12DR3B). d) Melt inclusion of type 2b originating from the resorption of a core antecryst (Sample 50DR1B).

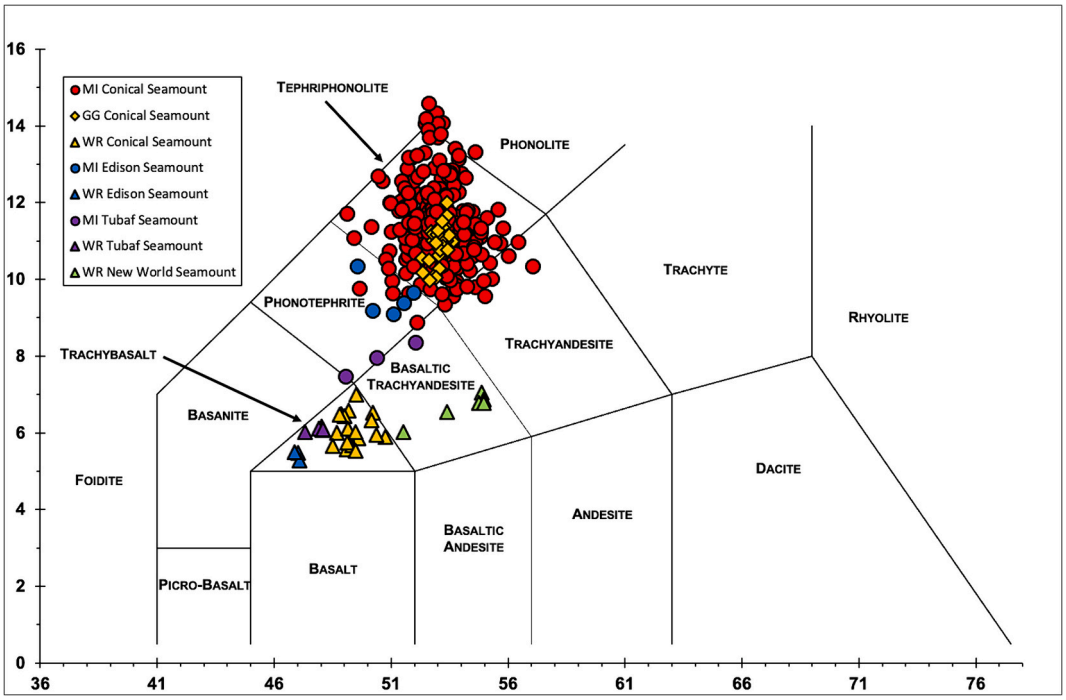

Fig. 7. *Total alkali* versus *silica (TAS) diagram* after Le Maitre et al. (2002). *Data shown include melt inclusions (MI, round symbols) from Conical (red), Edison (blue) and Tubaf seamounts (purple). Groundmass glass (GG) compositions from Conical Seamount (orange diamonds) and whole rock (WR; triangles) compositions from Conical (orange), Tubaf (blue), Edison (purple) and New World seamounts (green) are shown for comparison. The melt inclusions from Conical Seamount plot mainly in the tephriphonolitic domain, whereas the whole rock have a mostly trachybasaltic composition.* (For interpretation of the references to colour in this figure legend, the reader is referred to the web version of this article.)

elements than the other seamounts. Edison Seamount rocks (MgO = 7.7–7.9 wt%) are more depleted in HFSE (Nb, Ta, Zr, Hf) and in some REE (La, Ce, Pr, Er, Tm, Yb, Lu) but are relatively more enriched in Sm, Eu, Gd, Tb, and Dy. Conical Seamount (MgO = 4.5–6.7 wt%) is generally less enriched than the other seamounts in incompatible trace elements, except for some LILE (Cs, Rb), for which the contents overlap (Fig. 9a).

The melt inclusions and the groundmass glass at Conical Seamount show similar patterns compared to the whole rock samples. However,

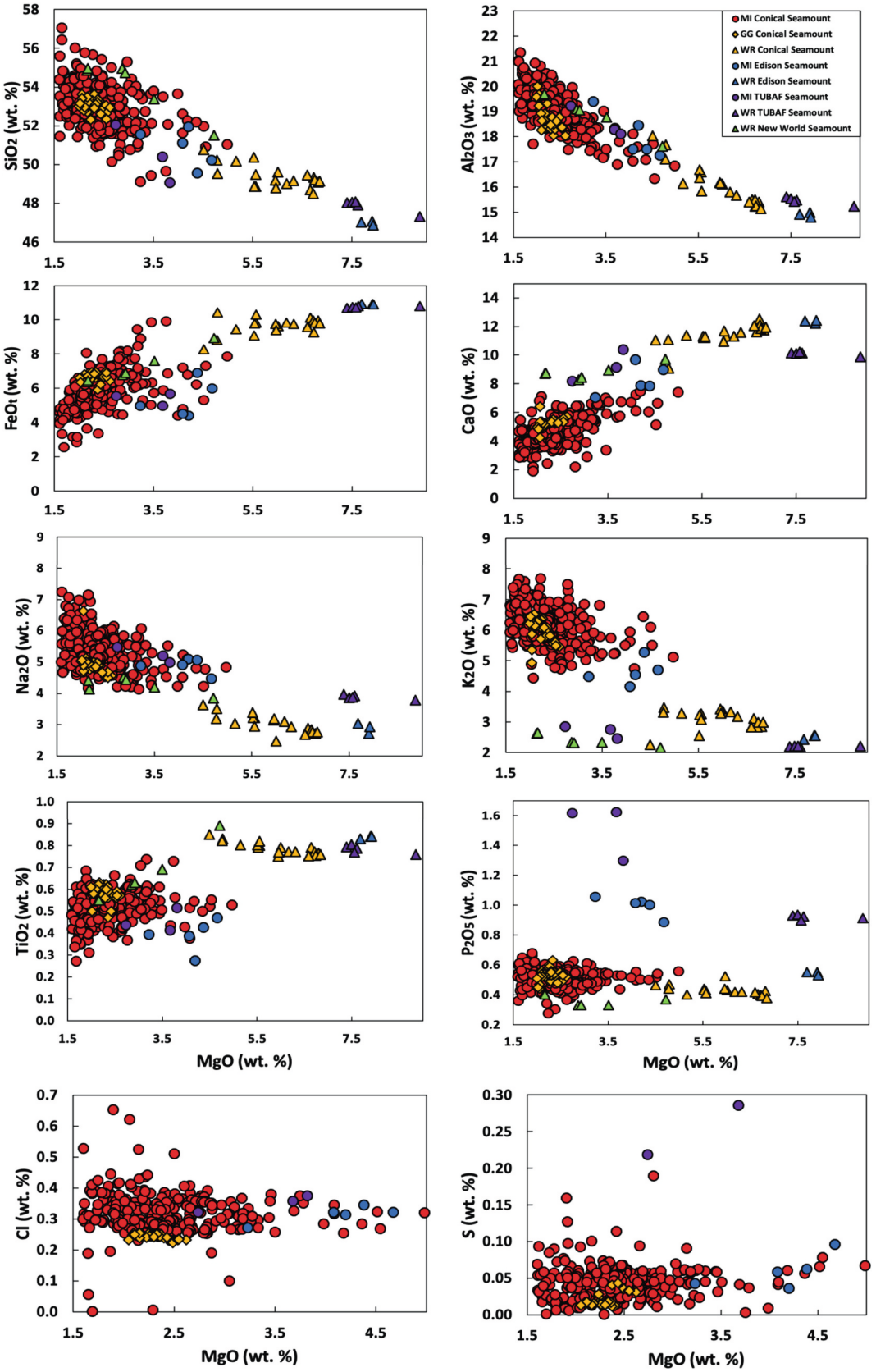

Fig. 8. Major element composition of whole rock samples (WR), groundmass glasses (GG) and melt inclusions in clinopyroxene (MI) from the Lihir seamounts. a) SiO_2, b) Al_2O_3, c) FeO_t, d) CaO, e) Na_2O, f) K_2O, g) TiO_2, h) P_2O_5, i) Cl and j) S versus MgO. Note that i) and j) include data of groundmass glass from Conical Seamount and melt inclusions from Conical, Tubaf and Edison seamounts only.

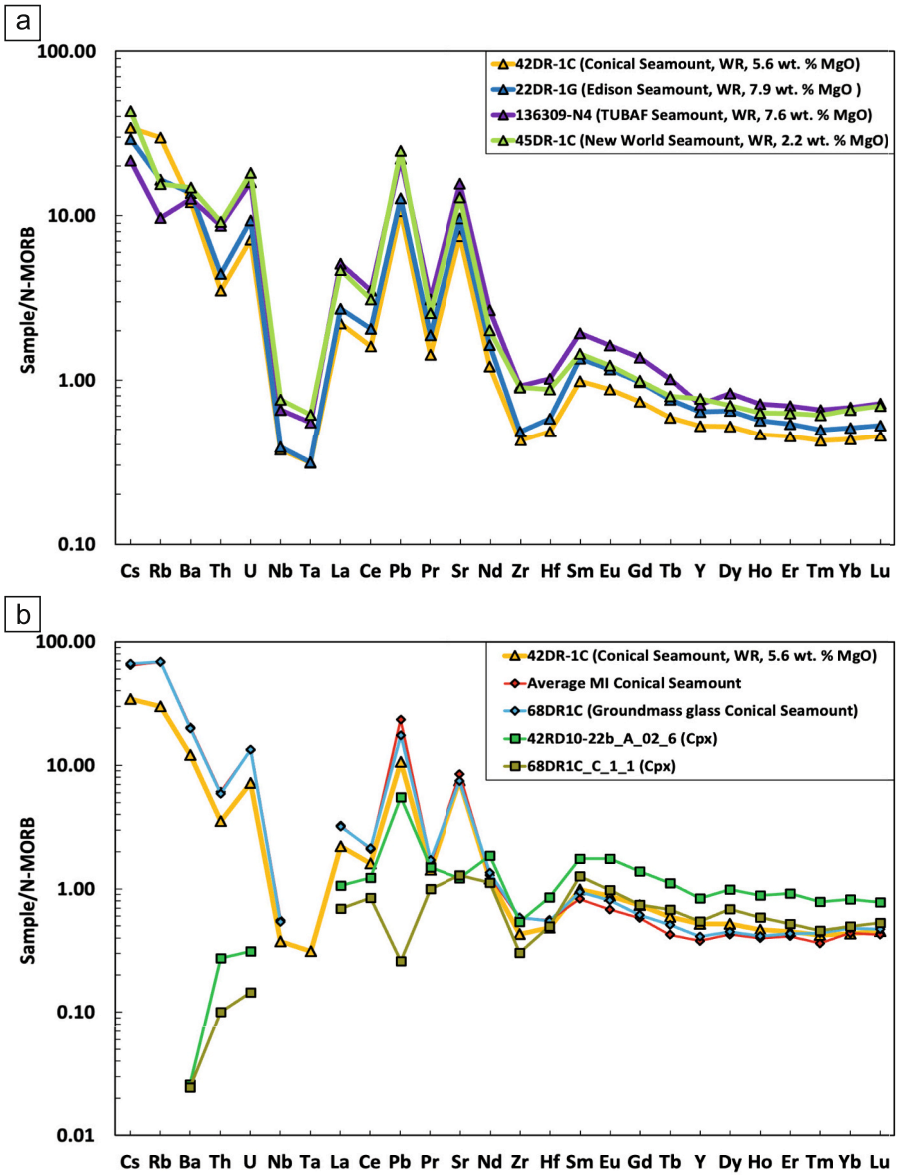

Fig. 9. Incompatible trace element composition normalized against the N-MORB composition of Gale et al. (2013). a) Representative whole rock samples from the seamounts around Lihir, b) Average compositions of groundmass glass and melt inclusions (MI) from Conical Seamount in comparison to representative whole rock composition sample 42DR-1C. The plot illustrates also two clinopyroxene compositions from Conical Seamount.

they are less enriched in some REE (Eu, Y, Gd, Tb, Dy, Ho, Er, Tm, Fig. 9b). Some melt inclusions are comparatively less enriched in some LILE (Sr, Ba, Fig. 9b). The clinopyroxene crystals hosting melt inclusions are depleted in almost all the elements except in some less incompatible REE (Eu, Y, Gd, Tb, Dy, Ho, Er, Tm, Yb, Lu).

Nb/Yb measured in the samples from Conical Seamount is close to N-MORB values (1.10 after Gale et al., 2013, Fig. 10a). However, Th/Yb measured in melt inclusions from Conical Seamount and in whole rock samples from Edison, New World, Tubaf and Conical seamounts varies between 0.2 and 1.5 (Fig. 10a) and is well above the ratio of N-MORB (0.08 after Gale et al., 2013). $(Dy/Yb)_N$ in whole rock samples from the studied Lihir seamounts are all below 1.5 (Fig. 10b). The ratio of Rb over Sr (Rb/Sr) in melt inclusions from Conical Seamount is higher than the whole rock composition and varies more with a range between 0.07 and 0.23 (Fig. 10c). Ratios of Ba/Rb for melt inclusions from Conical Seamount remain almost constant at MgO contents of 1.5 and 4.6 wt%, suggesting very similar parental melts supplying the magmatic system at Conical Seamount (Fig. 10d). The significantly higher Ba/Rb ranging between 8 and 18 in the samples from New World, Tubaf and Edison seamounts indicate distinct parental melts of these magmatic systems (Fig. 10d).

5. Discussion

5.1. Mantle sources and melting dynamics

While the TLTF island chain is not directly related to subduction, it is widely accepted that previous regional subduction episodes influenced the geochemical signature of the TLTF lavas (e.g., Kennedy et al., 1990). Comparatively high contents of trace elements that are mobilized in subduction zones either through fluids or melts (LILE, U, Th, Pb, La) indicate the addition of slab-derived components into the source (Stracke and Hegner, 1998). The displacement of the whole rock and melt inclusion composition to higher Th/Yb values compared to the MORB-OIB array from Pearce (2008) in the Th/Yb-Nb/Yb diagram (Fig. 10) is an additional evidence for subduction input (Pearce, 2008).

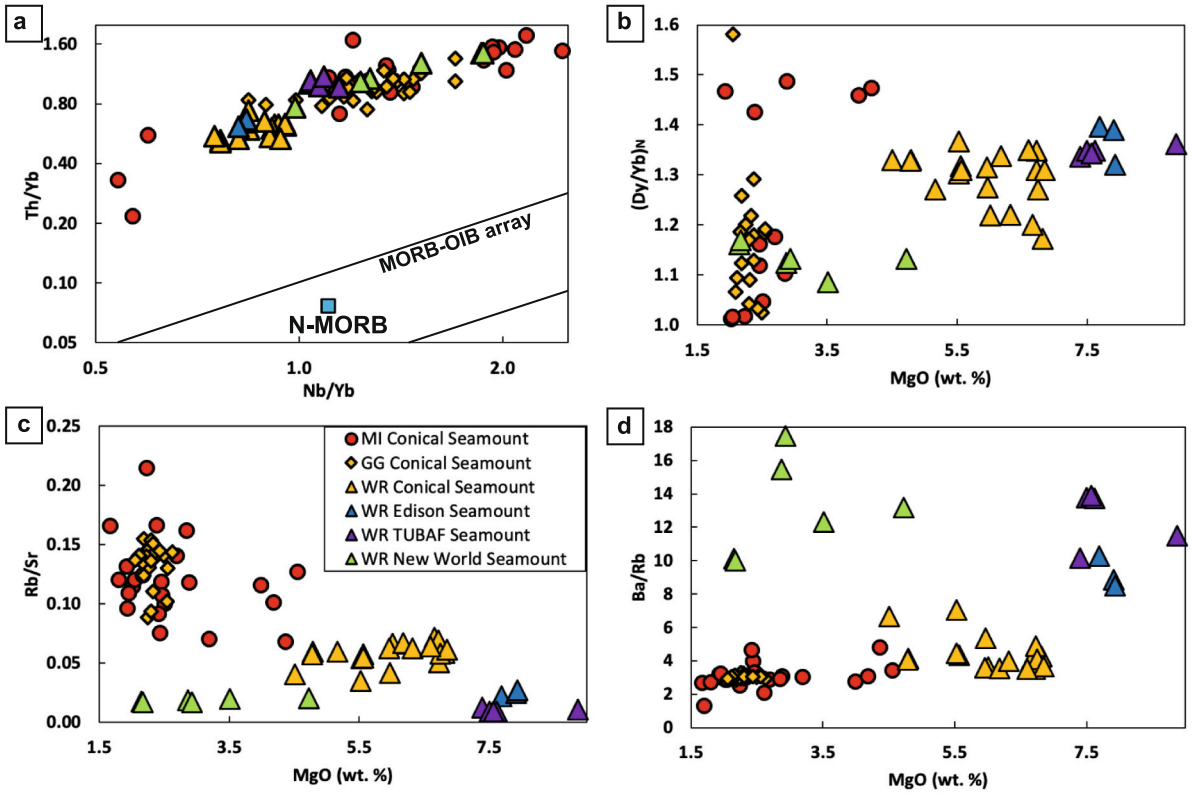

Fig. 10. Variations of a) Th/Yb versus Nb/Yb of melt inclusions from Conical Seamount and of whole rock samples from the seamounts around Lihir compared to N-MORB ratios after Gale et al. (2013) and the MORB-OIB array (marked by the two black lines) after Pearce (2008) b) $(Dy/Yb)_N$, chondrite-normalized after Mcdonough and Sun (1989), c) Rb/Sr and, d) Ba/Rb versus MgO in whole rock samples and melt inclusions from the seamounts around Lihir.

The low $(Dy/Yb)_N$ (below 1.5, Fig. 10b) measured in all samples indicates the absence of garnet in the mantle source (Davidson et al., 2013), which could retain HREE during melting. Elements considered to be "fluid-immobile", like HFSE and HREE compared to N-MORB, are depleted and indicate melting of mantle sources that were initially similar to or more depleted than the source of N-MORB (e.g., Pearce and Peate, 1995). Finally, this lower HREE content, combined with the plotting of Th/Yb versus Nb/Yb of the measured whole rock and melt inclusion compositions above the MORB-OIB array (Fig. 10), cannot be explained by single-stage melting process from an N-MORB mantle source.

In order to obtain further insights into the nature of these mantle sources and the partial melting processes, we performed geochemical modelling aiming at reproducing the contents of relatively fluid immobile elements (HFSE and HREE) in the most primitive TLTF rocks. We used the Depleted MORB Mantle (DMM) as the starting composition and the bulk partition coefficients of Workman and Hart (2004) in our modelling. We generated various melt-depleted sources from first-stage melting of the DMM by using variable degrees of partial melting ranging from 1 to 6%, (Workman and Hart, 2004). Second-stage melting of these sources with degrees of partial melting between 2 and 10% has been modelled using equations after Shaw (1970). The results of the modelling are shown in Fig. 1.

Melting of DMM reproduces the fluid-immobile HFSE (Nb, Ta, Hf, Zr) contents in the most primitive rocks of Conical, New World, Edison and Tubaf seamounts at 5–10% melting (Fig. 11a). However, our modelling predicts higher contents of HREE (Dy, Er, Yb) and Ti than in the natural TLTF rocks and their potential primary melt with presumably lower HREE content. Another possible scenario are very low degrees of partial melting (around 2%) of a previously depleted DMM source through 1–2% first-stage melting (Fig. 11b-c). However, this low degree of partial melting would also result in higher enrichment in HREE compared to TLTF lavas. A better fit of HREE and Ti is obtained through modelling of a 10% partial melt of a DMM source that was additionally depleted by 6% during a previous episode of melting (Fig. 11d). This finding is in agreement with previous studies that proposed the origin of TLTF parental magmas from a highly depleted mantle originally melted at a MOR spreading center (e.g., McInnes et al., 2001) followed by melting in an extensional regime within an ancient forearc basin (e.g., Kennedy et al., 1990). However, some elements (e.g., Nb, Ta) known to be fluid-immobile (e.g., Pearce and Peate, 1995) are significantly enriched in the lavas from the studied seamounts compared to model compositions. In order to resolve the apparent discrepancy between the model and observations, we propose that this HFSE enrichment might be linked to a transport of these elements in supercritical fluids, where HFSE are soluble like in silicate melts and therefore cannot be considered as perfectly fluid-immobile (Kessel et al., 2005). Such a scenario is consistent with extensive mantle metasomatism, source enrichment and alkali and volatile element increase by melt-like components (McInnes et al., 2001), probably as a consequence of the most recent subduction reversal in the region (e.g., Petterson et al., 1999).

The metasomatism of the mantle sources by melt-like K-rich subduction related components and low to moderate degrees of second-stage melting are the main causes of the high alkalinity of the TLTF magmas. This metasomatic enrichment overprints the first-stage melting depletion in incompatible trace elements. Results from our modelling point to a degree of second-stage melting between 5 and 10%. This range is consistent with the degree of partial melting inferred for other alkaline, trachybasaltic lavas in post-subduction settings (<10%, e.g., Hou et al., 2013).

The strong depletion in incompatible elements during first-stage melting is associated with Au enrichment in the residual mantle source (Richards, 2009). The second-stage melting of this residual mantle source promotes the transfer and enrichment of metals and

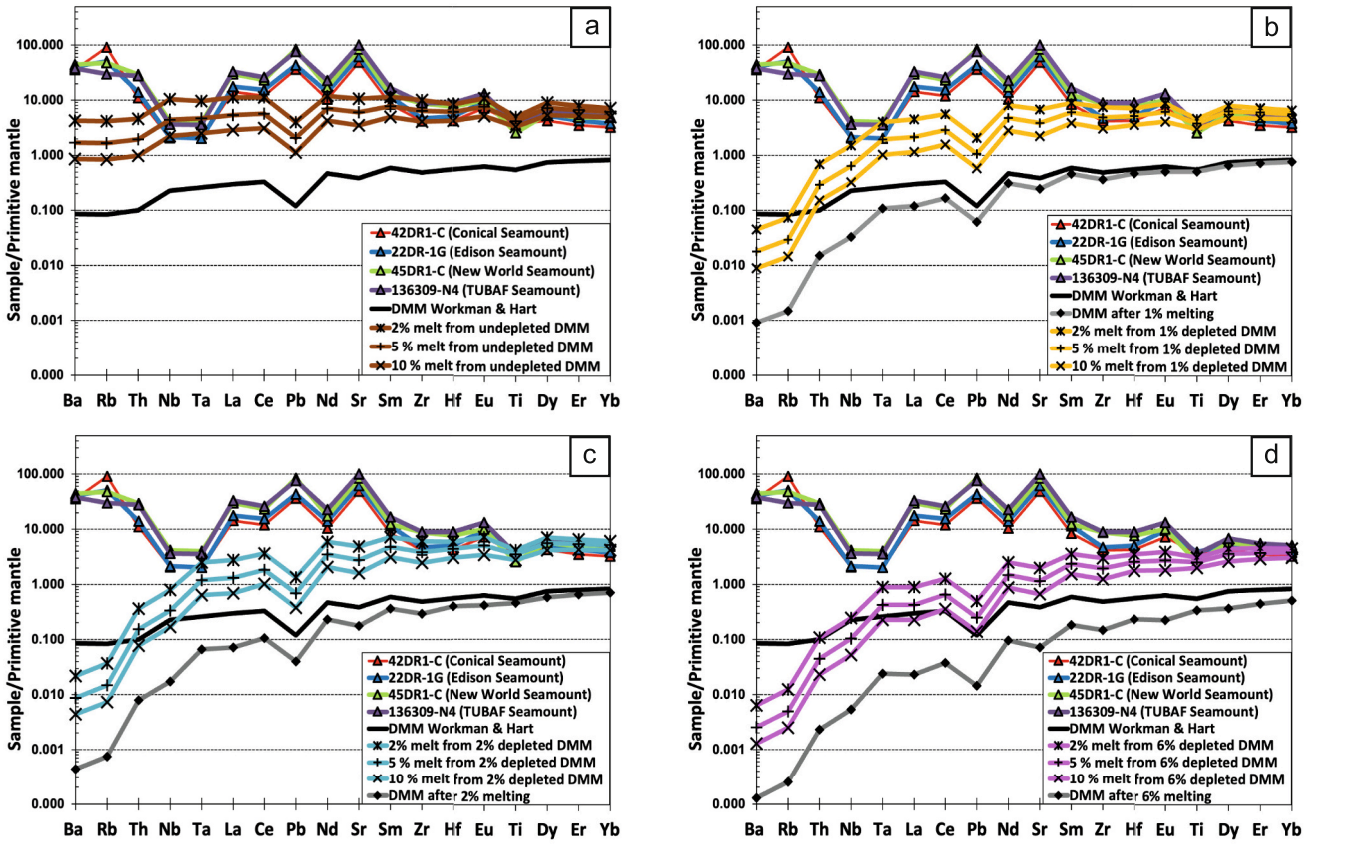

Fig. 11. Multi-element pattern of representative samples from the four main seamounts around Lihir, the DMM composition of Workman and Hart (2004) and modelled mantle source and melt compositions: a) Melt resulting from DMM without prior melting depletion b) after 1% melting depletion c) after 2% melting depletion d) after 6% melting depletion and of melt compositions after different degrees of partial melting (1%, 5%, 10%) from the different DMM scenarios. Trace element contents normalized to the primitive mantle of Lyubetskaya and Korenaga (2007).

volatiles in the TLTF magmatic systems (Holwell et al., 2019), which is an essential pre-requisite for ore formation.

5.2. A crustal magma chamber underneath Conical Seamount

Previous studies (Müller et al., 2003) suggested that the magmas from Conical, Tubaf and Edison seamounts start to crystallize at sub-crustal depths (10–14 kbar, around 32–46 km) in the stability field of amphibole, clinopyroxene and biotite. Beneath Conical Seamount, however, the initial differentiation stage is followed by further crystallization at upper crustal depths dominated by clinopyroxene and plagioclase, and in the presence of fluid phase (Kamenov et al., 2005). This scenario is also consistent with our petrographic observation of fluid inclusions commonly present in large clinopyroxene crystals of Conical Seamount lavas (Fig. 2b). The systematic presence of very large clinopyroxene crystals (up to several millimeters) in the rock samples indicate sustained magmatic activity in this shallow reservoir.

The similar magma evolution at depth between the melt batches supplying the magma chamber at Conical Seamount and the melts feeding Tubaf and Edison seamounts is further confirmed by the melt inclusion analysis: The major element compositions of melt inclusions from Tubaf and Edison seamounts mostly overlap with the least evolved melt inclusions from Conical Seamount.

The decrease of clinopyroxene-compatible elements (Ca) and increase of clinopyroxene-incompatible elements (Na, K, Al) in melts with decreasing MgO testify to clinopyroxene as the major fractionating phase for the late stage crystallization under Conical Seamount (cf. Stracke and Hegner, 1998). Additionally, melt inclusions have a lower content in HREE (Gd, Tb, Dy, Ho, Er, Tm, Yb) and Y compared to the whole rock composition. However, HREE and Y are relatively high and thus less incompatible in the analyzed clinopyroxene crystals. The higher compatibility of these elements in clinopyroxene phenocrysts from Conical Seamount can be explained by very high amount of Al^{IV} and Tschermak components in low Mg# clinopyroxene (Fig. 1). The high partition coefficient (D_{0REE}) for HREE in Tschermak-rich clinopyroxene is explained by coupled substitution of Ca—Si by REE-Al^{IV} (Mollo et al., 2020a; Wood and Trigila, 2001, Fig. 1). The lower HREE content in the more evolved melt inclusions compared to the more primitive whole rock composition is thus another indicator of the strong clinopyroxene fractionation at Conical Seamount.

Petrographic observations provide evidence for plagioclase crystallization along with clinopyroxene ±magnetite. Strontium is a compatible element in plagioclase. The average melt inclusion and the groundmass glass trace element pattern display similar or higher Sr content compared to the whole rock samples (Fig. 9). A systematic, strong plagioclase fractionation is therefore not evident from the trace element pattern observation. Additionally, the Al_2O_3 content increases with decreasing MgO (Fig. 8). Thus, the clinopyroxene crystallization dominates over plagioclase formation. However, the higher and more variable Rb/Sr of melt inclusions compared to whole rock samples indicates that variable amounts of plagioclase crystallized before each melt batch became trapped in the inclusion (Fig. 10c).

The presence of prominent core-rim zonation in clinopyroxene crystals, accompanied by resorption zones and sieve textures comprising glass inclusions (type 2), indicates repeated disequilibrium between crystals and the adjacent melt (Kamenov et al., 2005). Our new data confirm and refine these observations. The high Mg#'s, Cr_2O_3 contents and low Ts component in recurring clinopyroxene growth zones and

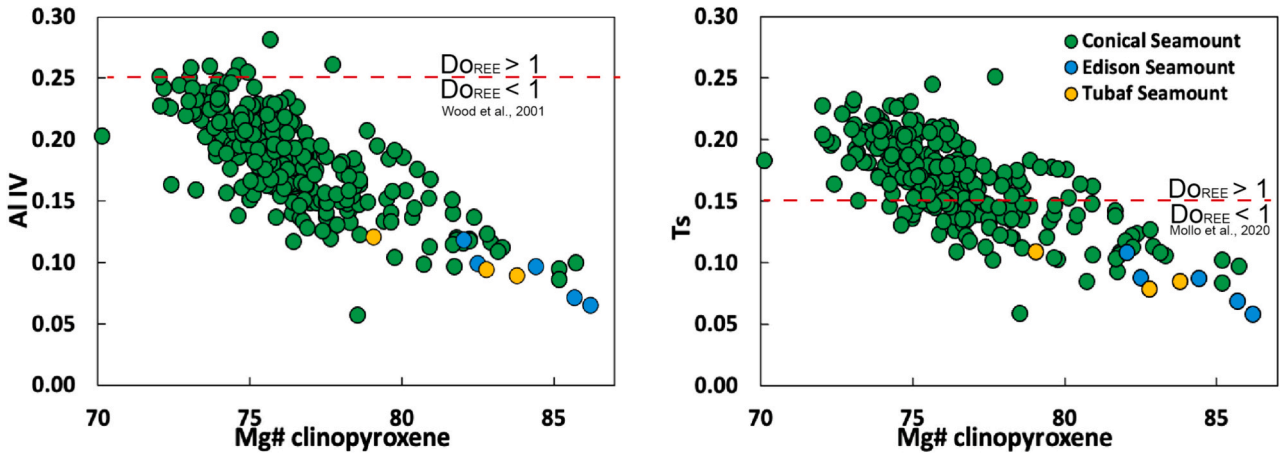

Fig. 12. Evolution of Al^{IV} and Tschermak (Ts) component depending on the Mg# of the clinopyroxene at Tubaf, Edison and Conical seamounts. The clinopyroxene-liquid strain free partition coefficient D_{0REE} is above 1 at higher Al^{IV} and Tschermak component (Mollo et al., 2020a; Wood and Trigila, 2001).

core zonation (Fig. 4) provide evidence for the repeated replenishment of more primitive, mafic magma likely carrying clinopyroxene antecrysts from deeper levels (Elardo and Shearer, 2014; Mollo et al., 2020b; Streck et al., 2002; Ubide and Kamber, 2018). They thus record numerous magma replenishment and mixing events in the magma chamber underneath Conical Seamount. The number of oscillatory zonation bands in individual crystals can range from one to at least four and indicates at least as many mixing and possibly replenishing events. Additionally, the reverse zoning found in some clinopyroxene crystals is consistent with the onset of a new crystal growth stage in the magma chamber where pre-existing minerals are overgrown and partially re-equilibrated in a more primitive (likely replenished) melt (Giacomoni et al., 2016).

The clinopyroxene glomerophyric intergrowths (Fig. 3) are additional evidence for cyclic fluctuations within the magma chamber. The density of the magma inferred from melt inclusion and bulk rock composition using DensityX (Iacovino and Till, 2019) ranges between 2.6 and 2.8 g/cm^3 for the most primitive and 2.3 to 2.5 g/cm^3 for the more differentiated compositions. These values are lower than clinopyroxene densities reported in the literature (around 3.3 g/cm^3, e.g., Lee, 2003). Therefore, the clinopyroxene crystals may tend to temporally settle and grow within stagnant melt in specific regions of the melt reservoir, likely at the bottom or the walls of the magma chamber. While this crystallization stage will favor radial, symmetric growth of glomerocrysts (Renjith, 2014), vigorous convection driven by the injection of hot primitive magma is required to expose the crystals to different melt batches. This process triggers new growth and finally leads to the formation of the stellar-like glomerophyric intergrowth observed in our samples (e.g., Zhu et al., 2018).

In contrast, plagioclase crystals have lower densities (between 2.5 and 2.6 g/cm^3, e.g., Scoates, 2000) and are more likely to float in melt or have neutral buoyancy. This is supported by the predominance of idiomorphic plagioclase and rare plagioclase within glomerophyric intergrowths. However, plagioclase crystals floating in a convecting melt are more prone to adhere together and to form the observed crystal cumulate textures (Renjith, 2014; Schwindinger, 1999; Vance, 1969, Fig. 3).

Additional, new evidence for repeated magma replenishment events beneath Conical Seamount with more primitive magmas arises from geochemistry. The melt inclusions from Conical Seamount record a large range in FeO_t and TiO2 contents (between 0.4 and 0.7 wt% TiO2 for MgO between 2.5 and 4.5 wt% and between 4.5 and 11 wt% FeO_t for MgO at 4.5 to 5.5 wt%). This variability, the significant decrease of Fe in the melt inclusions and the offset in TiO2 content between the melt inclusions and the whole rock compositions is consistent with the observed Ti-magnetite fractionation, replenishment of the magma chamber with more primitive Fe- and Ti-rich magma, and further mixing with low-Fe and low-Ti evolved melts in the magma chamber.

Thus, the observed clinopyroxene and plagioclase textures and compositions, and the compositions of melt inclusions in clinopyroxene suggest that the magmas erupted at Conical Seamount are the products of dynamic, convective magma chamber processes driven by frequent replenishment and mixing events. The presence of such a long-living and dynamic magma system is exclusive to the mineralized Conical Seamount but is missing at the other barren (not mineralized) seamounts nearby.

5.3. *Modelling magma chamber processes*

We used the Magma Chamber Simulator (Bohrson et al., 2020) in an attempt to quantitatively model the magma chamber evolution at Conical Seamount. Our simulations (Fig. 1) focused on fractional crystallization and the effects of periodic magma replenishments. We used the composition of the most primitive whole rock sample from Conical Seamount (sample 47DR-1 A) as the starting composition. To model anhydrous to significantly hydrous conditions, we considered three different H_2O contents in the parental melt of 0, 2 and 4 wt% and modelled isobaric crystallization trends at pressures varying from 50 MPa to 450 MPa in agreement with previous estimates of crystallization pressures (Müller et al., 2003). It agrees with the model of a crustal magma chamber underneath Conical Seamount experiencing fluid saturation as emphasized through our petrographic observations of fluid inclusions and previous research (Kamenov et al., 2005). Oxygen fugacity (fO_2) was set to vary between 0 and 2 log units above the Fayalite-Magnetite-Quartz (FMQ) buffer, which is a typical range for basaltic island arc magmas and their sources (e.g., Cottrell et al., 2021; Parkinson and Arculus, 1999).

There are several models with different input parameters that reproduce the observed trends in SiO_2, MgO, CaO, Na_2O, K_2O, and Al_2O_3 below 19 wt% (Fig. 1). In accordance with petrographic observations, all models predict prevailing clinopyroxene fractionation, as well as sequential olivine, magnetite, plagioclase, and apatite crystallization. Across our simulations, fractional crystallization of clinopyroxene dominated consistently, resulting in a final mass fraction of approximately 30–40%, aligning with the quantities observed in the natural rock samples. Only the clinopyroxene mass fraction from anhydrous simulations at a pressure of 450 MPa is significantly higher (45%). In all the scenarios, this extensive clinopyroxene fractionation drives the magma into very alkaline composition. Even though the alkalinity is a product of mantle source processes it is strongly enhanced by magma chamber processes.

At lower pressure of ~50 MPa and for fO_2 ranging between 0 and + 2

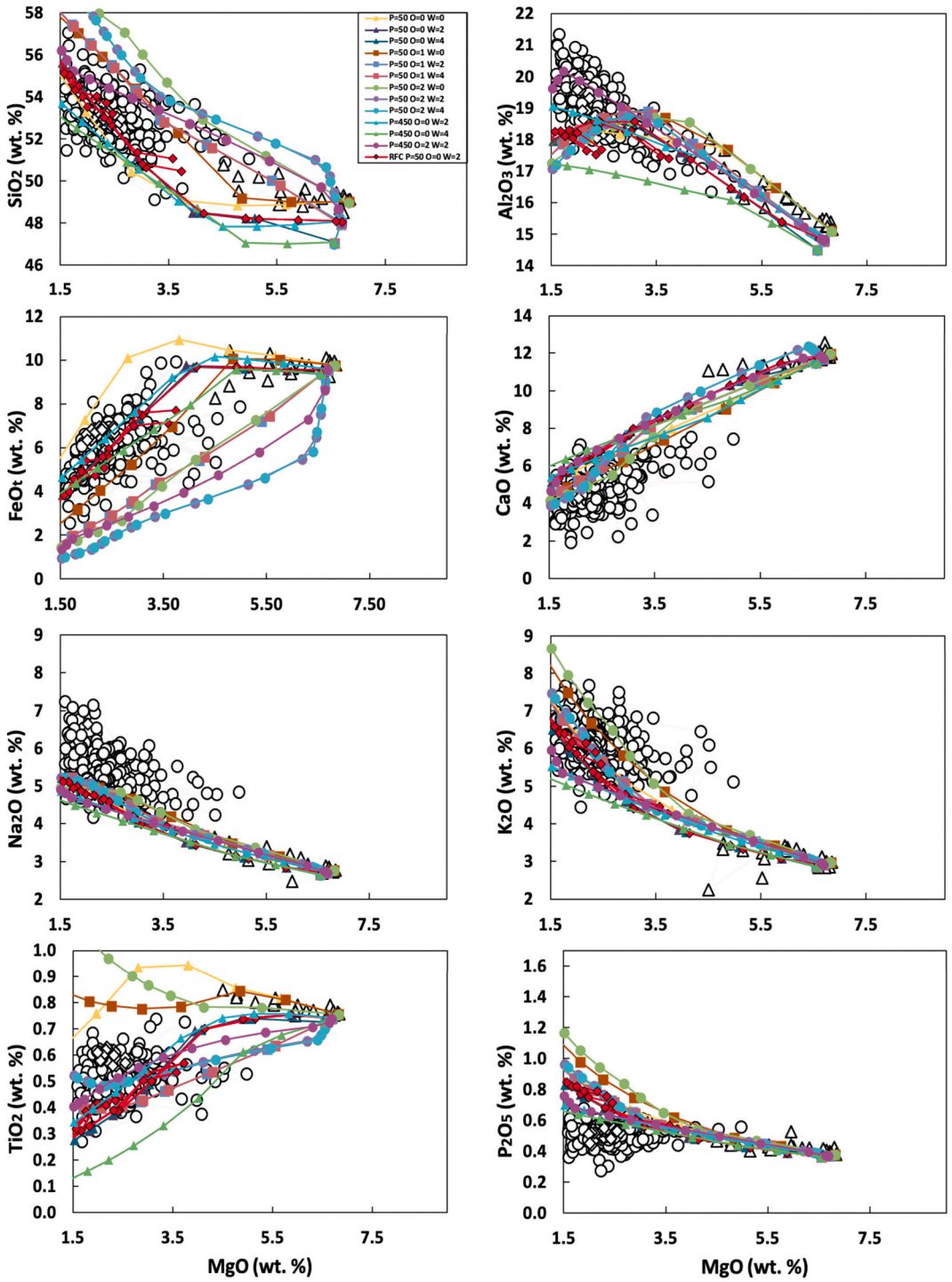

Fig. 13. Modelling of magma chamber evolution assuming different pressures, oxygen fugacity and H_2O contents (see text for details). Measurements (whole rock samples, groundmass glass and melt inclusions) are represented in white in the background (see Fig. 8 for more details). All models shown are isobaric at 50 MPa or 450 MPa. Different scenarios are labelled according to their pressure ("P" in MPa), oxygen fugacity ("O" in log units above FMQ buffer) and H_2O content ("W" in wt %). One additional scenario with fractional crystallization associated to several replenishing events (labelled 'RFC') is also plotted.

log units relative to FMQ, plagioclase mass fractions ranged between 21% and 27% for 4 wt% H_2O, between 22% and 41% for 2 wt% H_2O and between 38% and 44% for anhydrous conditions. Thus, models that ran at a higher pressure of ~450 MPa and assuming 2 to 4 wt% H_2O in the parental melt appear to be the most realistic as they predict a much lower amount of plagioclase (4–13 wt%) and are thus more consistent with our petrographic observations (5–10 area %). The modelled Al_2O_3, which is compatible in plagioclase, is thus closer to the measured melt inclusion composition.

Yet, the high Na_2O content at low MgO values is still not well reproduced at 450 MPa, despite a lower plagioclase fraction. In fact, the simulations at 450 MPa at 2 wt% and 4 wt% H_2O estimate an anorthite component between An_{51} to An_{80}. At Conical Seamount, the crystals have an anorthite component between An_{73} and An_{95}. The underestimation of the Anorthite component by the model, and thus overestimation of the Na_2O sequestrated in the plagioclase, explains the

discrepancy between Na_2O content modelled in the magma and measured in the melt inclusions. Previous experimental studies have shown the difficulty of magma modelling softwares to generate observed mineral assemblage in open, dynamic systems (Brugger and Hammer, 2010).

Despite this discrepancy, the different major element trends can be reproduced by several scenarios. However, the most critical data for the choice of the most appropriate conditions are those obtained for FeO_t and TiO_2, which are highly sensitive the crystallization of magnetite and linked to variations in fO_2. The most Fe- and Ti-rich melts can be reproduced only at relatively low fO_2 close to the FMQ buffer. Models at higher fO_2 predict early magnetite crystallization and very rapid depletion of Fe and Ti in melts with decreasing MgO. Thus, the large scatter of Fe and Ti in melts may reflect some variations in fO_2 during crystallization, broadly between 0 and + 2 log units relative to FMQ. However, such large variations in fO_2 for different melt batches are not well justified because the reasons for such large variation of fO_2 are unclear and not supported by our natural observations.

Before we have demonstrated that there is strong petrographic and geochemical evidence for periodic replenishment of the magma chamber. Thus, a realistic simulation of magma chamber evolution must include magma replenishment by mafic melts and mixing. However, most elements are largely unaffected by this additional process except for Fe and Ti, both of which exhibit non-monotonous behavior at decreasing MgO. Because this model involves mixing of high-Ti and high-Fe primitive and low-Ti and low-Fe evolved melts, it provides an alternative explanation for the large scatter of these elements at moderately low MgO and constant fO_2 close to the FMQ buffer as opposed to the model requiring variable fO_2 contents.

A mixing model seems likely because of the abundant evidence for magma mixing from petrographic and mineralogic data. However, the fO_2 close to FMQ predicted by the model is rather low compared to oxygen fugacity commonly accepted for arc-related magmas (e.g., Muth and Wallace, 2022). It is also below the range calculated from previous studies (0.7–2.5, Müller et al., 2003) at Conical Seamount. However, the oxybarometer, based on magnetite-melt equilibrium, used in Müller et al. (2003) is not calibrated for melts with high alkalinity like at Conical Seamount.

Based on the modelling results, we suggest that the magma fractionation occurred in a shallow magma chamber experiencing periodic replenishment, at fO_2 close to FMQ, and an H_2O content between 2 and 4 wt% in the parental melts. Additionally, we cannot completely exclude some uncertainty of the models as they may not be perfectly calibrated for applications in highly alkaline systems such as Conical Seamount.

5.4. Implications for the ore-forming potential at Conical Seamount

The Cu-Au-rich epithermal mineralization at Conical Seamount may have different genetic links to the underlying magmatic system: 1) Au enrichment at the source due to previous first-stage melting depletion (Richards, 2009) and subsequent transfer of metals and volatiles in highly alkaline melt during second-stage melting (Holwell et al., 2019), 2) pre-concentration of metals including Au in magmatic sulfides, 3) enrichment of the bulk magma in metals due to open-system fractionation and repeated replenishment by comparatively Au-rich mafic magmas, and 4) effective transfer of metals from the melt to the exsolving fluid due to volatile saturation.

The occurrence of magmatic sulfide phases is an important factor of ore metal pre-concentration because of their strong partitioning into sulfide phases (Li and Audétat, 2013). The Monosulfide Solid Solution (MSS) phase, for example, has MSS/silicate melt partition coefficients of up to 300 for Cu, 50 for Ag and 180 for Au (Li and Audétat, 2013). Sulfide liquids are even more enriched in these metals relative to silicate melts with partition coefficients of up to 800, 900 and 20,000 for Cu, Ag and Au (Li and Audétat, 2013). At Conical Seamount, Cu-bearing ISS phases are predominant among the magmatic sulfides. Measured Au and Ag contents in these magmatic sulfides reach 45 μg/g and 1397 μg/g, respectively, which are rather high (e.g., Li and Audétat, 2013).

The magmatic sulfides in lavas from Conical Seamount are genetically related to the crystallization of magnetite. Thus, their formation could be caused by a drop in the solubility of sulfide in the melt at decreasing FeO (O'Neill and Mavrogenes, 2002) and also by decreasing Fe_2O_3/FeO in melt, a process also known as "magnetite crisis" (Jenner et al., 2010). Therefore, a metal pre-concentration stage occurs through sulfide saturation and the gravitational retention of those sulfides in the chamber. Repeated periodic replenishing events delivering metals and sulfur, sulfide saturation and retention may thus lead to a progressive metal enrichment in the crustal magma reservoir. In the case of concomitant mixing in the magma chamber, sulfide phases likely remain in the partially crystallized magma either as small droplets in the melt or co-crystallized with minerals like magnetite. Thus, the sulfides are not removed from the magma, and their content in the bulk magma increases at relatively high MgO contents, similarly to highly incompatible elements (Lee et al., 2014; Portnyagin et al., 2015).

Another key feature for the ore-forming process is the fluid exsolution. Previous studies have demonstrated a substantial magmatic fluid contribution to the Cu—Au mineralization at Conical Seamount (e.g., Gemmell et al., 2004; Petersen et al., 2002). Since the main mineral phases crystallizing in the shallow magma chamber are exclusively anhydrous, fractional crystallization increases the volatile content in the melt and eventually triggers saturation and fluid exsolution (degassing). The broad range of Cl (mainly between 0.23 wt% and 0.45 wt%) and S contents (mainly between 0 wt% and 0.13 wt%) measured in melt inclusions is consistent with variable extent of melt degassing even though S is also affected by magmatic sulfide saturation. The high Cl content in the melt and equilibrium fluid increases metal solubility in the exsolving fluid (Hogg et al., 2023) and is an important factor for increasing the ore fertility of magmatic systems (Grondahl and Zajacz, 2022).

Volatile saturation and fluid exsolution may be an effective mechanism to extract magmatic sulfides from the convecting magma through the formation of sulfide-vapor compound droplets (Mungall et al., 2015). These compound droplets can ascend towards the roof of the magma chamber, where decomposition of the sulfide phase through hydration or oxidation can cause metals including Au to be transferred from the sulfide into the fluid phase, thus increasing the epithermal ore potential. However, the preservation of magmatic sulfides in the groundmass of the volcanic rock indicate that at Conical Seamount sulfides are at least not completely resorbed during degassing.

The presence of a crustal magma chamber may reflect an enhanced or enduring magmatic flux underneath Conical Seamount (cf. Gudmundsson, 2012). This conclusion is supported by the evidence for multiple magma replenishing events as well as the comparatively large size of Conical Seamount (2.3–2.9 km diameter, 700 m height) relative to Edison or Tubaf seamounts, both of which are around 1.1 km in diameter and only <400 m high (elevation above surrounding seafloor) and likely represent less complex edifices. Extensive fractionation of clinopyroxene in the magma chamber increases the alkalinity of the magma. This increased alkalinity potentially raises the pH of the ore-forming fluid, which enhances its capability to transport Au (Smith et al., 2017).

The parental melts for all seamounts around Lihir display compositional similarities and thus point to a similar mantle source. This source has been depleted in a first melting event which also increases Au over Cu. Low degrees of partial melting during a second event produces alkaline melts that initially fractionate at high pressures (e.g., at the Moho). However, this alone does not create favorable conditions for magmatic-hydrothermal ore formation: Edison, Tubaf and New World seamounts are barren (unmineralized), whereas an Au-rich epithermal mineralization is only known from Conical Seamount (Petersen et al., 2002). The presence of a shallow crustal magma reservoir that allows for extensive but complex magmatic differentiation, periodic replenishment, ore metal pre-enrichment and magmatic volatile saturation is

unique to Conical Seamount and appears to significantly increase magmatic-hydrothermal ore potentials.

6. Conclusions

Our investigation into the magmatic processes and their impact on the ore-forming system at Conical Seamount provides insights into the local mantle source, processes within the crustal magma chamber and the subsequent consequences for mineralization. Here, we summarize the key findings of our study:

1. Trace element modelling is consistent with a complex evolution of the mantle source that experienced two stages of depletion through partial melting and metasomatism in a supra-subduction setting. Metasomatism leads to enrichment in alkaline and volatile elements in the mantle source.
2. The depletion in incompatible elements during first-stage melting was associated to an enrichment in Au over Cu in the residual mantle source. The low to moderate degree of second-stage melting promotes the transfer of volatile and metal elements, the latter remained in the mantle source after the first melting depletion.
3. Geochemical analyses of melt inclusion indicate close compositional similarities between the melt batches supplying the magma chamber at Conical Seamount and the lavas observed at the neighboring Edison and Tubaf seamounts.
4. Our results from petrography, mineral and melt inclusions chemistry and modelling are consistent with magmatic differentiation at low pressure and under water-saturated conditions and provide evidence for frequent magma replenishment events and dynamic convection in the magma chamber.
5. The presence of magmatic sulfides provides evidence for sulfide saturation in the magma and the sequestration of metals in the sulfide phase. Cyclic replenishment and convection of the magma chamber provide a fertile environment for a progressive metal enrichment through retention of the sulfides in the residual magma.
6. Our study highlights the important role of a shallow crustal reservoir for magmatic-hydrothermal ore formation. Extensive fractionation of clinopyroxene increases the alkalinity and volatile content of the magma. Upon volatile saturation, the exsolving fluid has a high potential to mobilized and transport metals, thus creating highly favorable conditions for an epithermal ore system.
7. Conical Seamount is the only seamount in the region with solid evidence for the enduring presence of a shallow crustal magma reservoir. Our results may thus explain why Cu—Au mineralization at the seafloor of the New Ireland Basin is unique to this location.

We suggest that mantle source and parental melt composition play an important but limited role for the ore metal enrichment in highly alkaline magmas and thus for their magmatic-hydrothermal mineral potentials in general. In contrast, our study shows that magma evolution and shallow crustal magma chamber processes including periodic melt replenishment control sulfide and magmatic volatile saturation and as such play a critical role for epithermal ore formation.

CRediT authorship contribution statement

Louis-Maxime Gautreau: Conceptualization, Formal analysis, Investigation, Methodology, Software, Visualization, Writing – original draft, Writing – review & editing. **Thor H. Hansteen:** Conceptualization, Methodology, Project administration, Resources, Supervision, Validation, Writing – review & editing. **Maxim Portnyagin:** Conceptualization, Methodology, Validation, Writing – review & editing. **Christoph Beier:** Conceptualization, Formal analysis, Methodology, Validation, Writing – review & editing. **Matthias Frische:** Formal analysis, Methodology, Writing – review & editing. **Philipp A. Brandl:** Conceptualization, Funding acquisition, Methodology, Project administration, Resources, Supervision, Validation, Writing – review & editing.

Declaration of Generative AI and AI-assisted technologies in the writing process.

Statement: During the preparation of this work the author(s) used ChatGPT in order to check only grammatic and idiomatic correctness of the already written manuscript to improve language and readability. After using this tool/service, the author(s) reviewed and edited the content as needed and take(s) full responsibility for the content of the publication.

Declaration of Competing Interest

The authors declare that they have no known competing financial interests or personal relationships that could have appeared to influence the work reported in this paper.

Acknowledgements

This study is funded by the German Research Foundation (DFG) through grant BR 5297/4-1 in the DOME priority program. A special thanks is given to Sven Petersen and Colin Devey for their valued advice and support, as well as to Mario Thöner (all GEOMAR) for his valuable help during the electron microprobe analyses. We acknowledge the help and support of Marcel Regelous (FAU Erlangen-Nürnberg), Dieter Garbe-Schönberg and Ulrike Westernströer (both CAU Kiel) during ICPMS analysis and Andreas Stracke (University of Münster) for providing SO94 sample material. We thank Richard Arculus for providing SHAARC cruise sample material and Antoine Bénard (both ANU) for help during preparation of the samples.

Appendix A. Supplementary data

Supplementary data to this article can be found online at https://doi.org/10.1016/j.lithos.2024.107695.

References

Abbott, L.D., 1995. Neogene tectonic reconstruction of the Adelbert-Finisterre-New Britain collision, northern Papua New Guinea. J. SE Asian Earth Sci. 11, 33–51. https://doi.org/10.1016/0743-9547(94)00032-A.

Baldwin, S.L., Fitzgerald, P.G., Webb, L.E., 2012. Tectonics of the new Guinea region. Annu. Rev. Earth Planet. Sci. 40, 495–520. https://doi.org/10.1146/annurev-earth-040809-152540.

Bénard, A., Müntener, O., Pilet, S., Arculus, R.J., Nebel, O., 2021. Silica-rich spinel harzburgite residues formed by fractional hybridization-melting of the intra-oceanic supra-subduction zone mantle: New evidence from TUBAF seamount peridotites. Geochim. Cosmochim. Acta 293, 477–506. https://doi.org/10.1016/j.gca.2020.11.001.

Bohrson, W.A., Spera, F.J., Heinonen, J.S., Brown, G.A., Scruggs, M.A., Adams, J.V., Takach, M.K., Zeff, G., Suikkanen, E., 2020. Diagnosing open-system magmatic processes using the Magma Chamber Simulator (MCS): part I—major elements and phase equilibria. Contrib. Mineral. Petrol. 175, 1–29. https://doi.org/10.1007/s00410-020-01722-z.

Brandl, P.A., Hannington, M.D., Geersen, J., Petersen, S., Gennerich, H.H., 2020. The submarine tectono-magmatic framework of Cu-au endowment in the Tabar-to-Feni island chain. PNG. Ore Geol. Rev. 121, 103491 https://doi.org/10.1016/j.oregeorev.2020.103491.

Brugger, C.R., Hammer, J.E., 2010. Crystallization kinetics in continuous decompression experiments: Implications for interpreting natural magma ascent processes. J. Petrol. 51, 1941–1965. https://doi.org/10.1093/petrology/egq044.

Cooke, D.R., Sykora, S., Lawlis, E., Blackwell, J.L., Ageneau, M., Jansen, N.H., Harris, A. C., Selley, D., 2020. Chapter 28: Lihir Alkalic Epithermal Gold Deposit. Papua New Guinea. Geol. World's Major Gold Depos. Prov. 579–597. https://doi.org/10.5382/sp.23.28.

Cottrell, E., Birner, S.K., Brounce, M., Davis, F.A., Waters, L.E., Kelley, K.A., 2021. Oxygen fugacity across tectonic settings. Geophysical Monograph Series. 33–61.

Davidson, J., Turner, S., Plank, T., 2013. Dy/Dy*: Variations arising from mantle sources and petrogenetic processes. J. Petrol. 54, 525–537. https://doi.org/10.1093/petrology/egs076.

Davies, R.H., Ballantyne, G.H., 1987. Geology of the Ladolam gold deposit Lihir Island, Papua New Guinea. In: Pacific Rim Congress. Gold Coast Queensland, Australia, pp. 943–949.
Duke, J.M., 1976. Distribution of the period four transition elements among olivine, calcic clinopyroxene and mafic silicate liquid: Experimental results. J. Petrol. 17, 499–521. https://doi.org/10.1093/petrology/17.4.499.
Elardo, S.M., Shearer, C.K., 2014. Magma chamber dynamics recorded by oscillatory zoning in pyroxene and olivine phenocrysts in basaltic lunar meteorite Northwest Africa 032. Am. Mineral. 99, 355–368. https://doi.org/10.1515/am.2014.4552.
Exon, N.F., Marlow, M.S., 1988. Geology and offshore resource potential of the New Ireland-Manus Region - A Synthesis. In: Marlow, M.S., Dadisman, S.V., Exon, N.F. (Eds.), Geology and Offshore Resources of Pacific Island Arcs - New Ireland and Manus Region, Papua New Guinea. Circum-Pacific Council for Energy and Mineral Resources Earth Science Series 9. Circum-Pacific Council for Energy and Mineral Resources, Houston.
Franz, L., Romer, R.L., 2010. Different styles of metasomatic veining in ultramafic xenoliths from the TUBAF Seamount (Bismarck Microplate, Papua New Guinea). Lithos 114, 30–53. https://doi.org/10.1016/j.lithos.2009.07.013.
Gale, A., Dalton, C.A., Langmuir, C.H., Su, Y., Schilling, J.G., 2013. The mean composition of ocean ridge basalts. Geochem. Geophys. Geosyst. https://doi.org/10.1029/2012GC004334.
Gemmell, J.B., Sharpe, R., Jonasson, I.R., Herzig, P.M., 2004. Sulfur Isotope Evidence for Magmatic Contributions to Submarine and Subaerial Gold Mineralization : Conical Seamount and the Ladolam Gold Deposit, Papua New Guinea. Econ. Geol. 99, 1711–1725.
Georgatou, A.A., Chiaradia, M., 2020. Magmatic sulfides in high-potassium calc-alkaline to shoshonitic and alkaline rocks. Solid Earth 11, 1–21. https://doi.org/10.5194/se-11-1-2020.
Giacomoni, P.P., Coltorti, M., Bryce, J.G., Fahnestock, M.F., Guitreau, M., 2016. Mt. Etna plumbing system revealed by combined textural, compositional, and thermobarometric studies in clinopyroxenes. Contrib. Mineral. Petrol. 171, 1–15. https://doi.org/10.1007/s00410-016-1247-7.
Grondahl, C., Zajacz, Z., 2022. Sulfur and chlorine budgets control the ore fertility of arc magmas. Nat. Commun. 13, 1–11. https://doi.org/10.1038/s41467-022-31894-0.
Gudmundsson, A., 2012. Magma chambers: Formation, local stresses, excess pressures, and compartments. J. Volcanol. Geotherm. Res. 237–238, 19–41. https://doi.org/10.1016/j.jvolgeores.2012.05.015.
Hammarstrom, J., Bookstrom, A., Dicken, C., Drenth, B., Ludington, S., Robinson, G., Setiabudi, B., Sukserm, W., Sunuhadi, N., YanSzeWah, A., Zientek, M., 2013. Porphyry Copper Assessment of Southeast Asia and Melanesia. Glob. Miner. Resour, Assess, p. 352.
Herzig, P.M., 2002. Cruise Report SO-166: Detailed Investigation of the Magmatic-Hydrothermal Gold Mineralization at Conical Seamount (New Ireland Basin) and of Massive Sulfides at PACMANUS (Eastern Manus Basin) (Papua New Guinea by Shallow Drilling).
Herzig, P.M., Hannington, M.D., Stoffers, P., Arribas, A., Becker, K.-P., Binns, R., Browne, P., Gennerich, H.-H., Hartmann, M., Heesemann, B., Hefter, J., Jonasson, I., Kila, R., Lange, S., McInnes, B.I.A., Meyers, J., Percival, J., Petersen, S., Pichler, T., Rosenberger, A., Ruggieri, G., Schott, T., Schwarz, U., Seifert, R., Villinger, H., Winn, K., 1994. Cruise Report Sonne-94: Tectonics, Petrology and Hydrothermal Processes in Areas of Alkaline Island-Arc Volcanoes in the Southwest Pacific.
Herzig, P., Hannington, M., Stoffers, P., Becker, K., Drischel, M., Franz, L., Gemmell, B., Höppner, B., Kia, P., Mühlhan, N., Nickelsen, S., Percival, J., Perfit, M., 1998. Cruise Report SO-133: Volcanism, Hydrothermal Processes and Bilogical Communities at Shallow Submarine Volcanoes of the New Ireland Fore-Arc (Papua New Guinea).
Hogg, O.R., Edmonds, M., Blundy, J., 2023. Water-rich magmas optimise volcanic chalcophile element outgassing fluxes. Earth Planet. Sci. Lett. 611, 118153 https://doi.org/10.1016/j.epsl.2023.118153.
Holm, R.J., Spandler, C., Richards, S.W., 2015. Continental collision, orogenesis and arc magmatism of the Miocene Maramuni arc. Papua New Guinea. Gondwana Res. 28, 1117–1136. https://doi.org/10.1016/j.gr.2014.09.011.
Holm, R.J., Tapster, S., Jelsma, H.A., Rosenbaum, G., Mark, D.F., 2019. Tectonic evolution and copper-gold metallogenesis of the Papua New Guinea and Solomon Islands region. Ore Geol. Rev. 104, 208–226. https://doi.org/10.1016/j.oregeorev.2018.11.007.
Holwell, D.A., Fiorentini, M., McDonald, I., Lu, Y., Giuliani, A., Smith, D.J., Keith, M., Locmelis, M., 2019. A metasomatized lithospheric mantle control on the metallogenic signature of post-subduction magmatism. Nat. Commun. 10, 1–10. https://doi.org/10.1038/s41467-019-11065-4.
Horz, K.H., Worthington, T.J., Winn, K., Stoffers, P., 2004. Late Quaternary tephra in the New Ireland Basin, Papua New Guinea. J. Volcanol. Geotherm. Res. 132, 73–95. https://doi.org/10.1016/S0377-0273(03)00421-9.
Hou, Z., Zheng, Y., Yang, Z., Rui, Z., Zhao, Z., Jiang, S., Qu, X., Sun, Q., 2013. Contribution of mantle components within juvenile lower-crust to collisional zone porphyry Cu systems in Tibet. Mineral. Deposita 48, 173–192. https://doi.org/10.1007/s00126-012-0415-6.
Iacovino, K., Till, C.B., 2019. DensityX: a program for calculating the densities of magmatic liquids up to 1,627 °C and 30 kbar. Volcanica 2, 1–10.
Jenner, F.E., O'Neill, H.S.C., Arculus, R.J., Mavrogenes, J.A., 2010. The magnetite crisis in the evolution of arc-related magmas and the initial concentration of au, Ag and Cu. J. Petrol. 51, 2445–2464. https://doi.org/10.1093/petrology/egq063.
Kamenov, G.D., Perfit, M.R., Jonasson, I.R., Mueller, P.A., 2005. High-precision Pb isotope measurements reveal magma recharge as a mechanism for ore deposit formation: examples from Lihir Island and Conical seamount, Papua New Guinea. Chem. Geol. 219, 131–148. https://doi.org/10.1016/j.chemgeo.2005.02.013.
Kennedy, A.K., Hart, S.R., Frey, F.A., 1990. Composition and isotopic constraints on the petrogenesis of alkaline arc lavas: Lihir Island, Papua New Guinea. J. Geophys. Res. 95, 6929–6942. https://doi.org/10.1029/JB095iB05p06929.
Kessel, R., Schmidt, M.W., Ulmer, P., Pettke, T., 2005. Trace element signature of subduction-zone fluids, melts and supercritical liquids at 120-180 km depth. Nature 437, 724–727. https://doi.org/10.1038/nature03971.
Klügel, A., Klein, F., 2006. Complex magma storage and ascent at embryonic submarine volcanoes from the Madeira Archipelago. Geology 34, 337–340. https://doi.org/10.1130/G22077.1.
Le Maitre, R.W., Bateman, P., Dudek, A., Keller, J., Lameyre Le Bas, M.J., Sabine, P.A., Schmid, R., Sorensen, H., Streckeisen, A., Woodley, A.R., Zanetti, B., 2002. Igneous Rocks (A classification and glossary of terms).
Lee, C.-T.A., 2003. Compositional variation of density and seismic velocities in natural peridotites at STP conditions: Implications for seismic imaging of compositional heterogeneities in the upper mantle. J. Geophys. Res. Solid Earth 108. https://doi.org/10.1029/2003jb002413.
Lee, C.T.A., Lee, T.C., Wu, C.T., 2014. Modeling the compositional evolution of recharging, evacuating, and fractionating (REFC) magma chambers: Implications for differentiation of arc magmas. Geochim. Cosmochim. Acta 143, 8–22. https://doi.org/10.1016/j.gca.2013.08.009.
Li, Y., Audétat, A., 2013. Gold solubility and partitioning between sulfide liquid, monosulfide solid solution and hydrous mantle melts: Implications for the formation of Au-rich magmas and crust-mantle differentiation. Geochim. Cosmochim. Acta 118, 247–262. https://doi.org/10.1016/j.gca.2013.05.014.
Licence, P.S., Terrill, J.E., Fergusson, L.J., 1987. Epithermal Gold Mineralisation, Ambitle Island, Papua New Guinea, in: Pacific Rim Congress. Gold Coast Queensland, Australia.
Lyubetskaya, T., Korenaga, J., 2007. Chemical composition of Earth's primitive mantle and its variance: 1. Method and results. J. Geophys. Res. 112, 1–21.
Mann, P., Taira, A., 2004. Global tectonic significance of the Solomon Islands and Ontong Java Plateau convergent zone. Tectonophysics 389, 137–190. https://doi.org/10.1016/j.tecto.2003.10.024.
Mcdonough, W.F., Sun, S.S., 1989. Chemical and isotopic systematics of oceanic basalts: Implications for mantle composition and processes. Geol. Soc. Spec. Publ. 42, 313–345. https://doi.org/10.1144/GSL.SP.1989.042.01.19.
McInnes, B.I.A., 1992. A Glimpse of Ephemeral Subduction Zone Processes from Simberi Island. Papua New Guinea.
Mcinnes, B.I.A., Arculus, R., Massoth, G., Baker, E., Deronde, C., Mcconachy, T., Posai, P., 2000. Project SHAARC: Investigation of Submarine, Hydrothermally Active ARC Volcanoes in the and By.
McInnes, B.I.A., Gregoire, M., Binns, R.A., Herzig, P.M., Hannington, M.D., 2001. Hydrous metasomatism of oceanic sub-arc mantle, Lihir, Papua New Guinea: Petrology and geochemistry of fluid-metasomatised mantle wedge xenoliths. Earth Planet. Sci. Lett. 188, 169–183. https://doi.org/10.1016/S0012-821X(01)00306-5.
Mollo, S., Blundy, J., Scarlato, P., Vetere, F., Holtz, F., Bachmann, O., Gaeta, M., 2020a. A review of the lattice strain and electrostatic effects on trace element partitioning between clinopyroxene and melt: applications to magmatic systems saturated with Tschermak-rich clinopyroxenes. Earth-Science Rev. 210, 103351 https://doi.org/10.1016/j.earscirev.2020.103351.
Mollo, S., Ubide, T., Di Stefano, F., Nazzari, M., Scarlato, P., 2020b. Polybaric/polythermal magma transport and trace element partitioning recorded in single crystals: a case study of a zoned clinopyroxene from Mt. Etna. Lithos 356–357, 105382. https://doi.org/10.1016/j.lithos.2020.105382.
Moyle, A.J., Doyle, B.J., Hoogvliet, H., Ware, A.R., 1990. Ladolam gold deposit, Lihir Island: Australian Institute of Mining and Metallurgy Monograph, 14, pp. 1793–1805.
Müller, D., Franz, L., Petersen, S., Herzig, P.M., Hannington, M.D., 2003. Comparison between magmatic activity and gold mineralization at Conical Seamount and Lihir Island, Papua New Guinea. Mineral. Petrol. 79, 259–283. https://doi.org/10.1007/s00710-003-0007-3.
Mungall, J.E., Brenan, J.M., Godel, B., Barnes, S.J., Gaillard, F., 2015. Transport of metals and Sulphur in magmas by flotation of sulphide melt on vapour bubbles. Nat. Geosci. 8, 216–219. https://doi.org/10.1038/ngeo2373.
Muth, M.J., Wallace, P.J., 2022. Sulfur Recycling in Subduction Zones and the Oxygen Fugacity of Mafic Arc Magmas. Earth Planet. Sci, Lett, p. 599.
O'Neill, H.S.C., Mavrogenes, J.A., 2002. The sulfide capacity and the sulfur content at sulfide saturation of silicate melts at 1400°C and 1 bar. J. Petrol. 43, 1049–1087. https://doi.org/10.1093/petrology/43.6.1049.
Parkinson, I.J., Arculus, R.J., 1999. The redox state of subduction zones: Insights from arc-peridotites. Chem. Geol. 160, 409–423. https://doi.org/10.1016/S0009-2541(99)00110-2.
Pearce, J.A., 2008. Geochemical fingerprinting of oceanic basalts with applications to ophiolite classification and the search for Archean oceanic crust. Lithos 100, 14–48. https://doi.org/10.1016/j.lithos.2007.06.016.
Pearce, J.A., Peate, D.W., 1995. Tectonic Implications of the Composition of Volcanic Arc Magmas. Annu. Rev. Earth Planet. Sci.
Petersen, S., Herzig, P.M., Hannington, M.D., Jonasson, I.R., 2002. Submarine Gold Mineralization near Lihir Island. New Ireland Fore-Arc, Papua New Guinea 97, 1795–1813.
Petterson, M.G., Babbs, T., Neal, C.R., Mahoney, J.J., Saunders, A.D., Duncan, R.A., Tolia, D., Magu, R., Qopoto, C., Mahoa, H., Natogga, D., 1999. Geological-tectonic framework of Solomon Islands, SW Pacific: Crustal accretion and growth within an intra-oceanic setting. Tectonophysics 301, 35–60. https://doi.org/10.1016/S0040-1951(98)00214-5.
Portnyagin, M., Duggen, S., Hauff, F., Mironov, N., Bindeman, I., Thirlwall, M., Hoernle, K., 2015. Geochemistry of the late Holocene rocks from the Tolbachik

volcanic field, Kamchatka: Quantitative modelling of subduction-related open magmatic systems. J. Volcanol. Geotherm. Res. 307, 133–155. https://doi.org/10.1016/j.jvolgeores.2015.08.015.
Putirka, K.D., 2008. Thermometers and barometers for volcanic systems. Rev. Mineral. Geochem. 69, 61–120. https://doi.org/10.2138/rmg.2008.69.3.
Renjith, M.L., 2014. Micro-textures in plagioclase from 1994-1995 eruption, Barren Island Volcano: evidence of dynamic magma plumbing system in the Andaman subduction zone. Geosci. Front. 5, 113–126. https://doi.org/10.1016/j.gsf.2013.03.006.
Renno, A.D., Franz, L., Witzke, T., Herzig, P.M., 2004. The coexistence of melts of hydrous copper chloride, sulfide and silicate compositions in a magnesiohastingsite cumulate, TUBAF Seamount, Papua New Guinea. Can. Mineral. 42, 1–16. https://doi.org/10.2113/gscanmin.42.1.1.
Richards, J.P., 2009. Postsubduction porphyry Cu-au and epithermal au deposits: Products of remelting of subduction-modified lithosphere. Geology 37, 247–250. https://doi.org/10.1130/G25451A.1.
Rose-Koga, E.F., Bouvier, A.S., Gaetani, G.A., Wallace, P.J., Allison, C.M., Andrys, J.A., Angeles de la Torre, C.A., Barth, A., Bodnar, R.J., Bracco Gartner, A.J.J., Butters, D., Castillejo, A., Chilson-Parks, B., Choudhary, B.R., Cluzel, N., Cole, M., Cottrell, E., Daly, A., Danyushevsky, L.V., DeVitre, C.L., Drignon, M.J., France, L., Gaborieau, M., Garcia, M.O., Gatti, E., Genske, F.S., Hartley, M.E., Hughes, E.C., Iveson, A.A., Johnson, E.R., Jones, M., Kagoshima, T., Katzir, Y., Kawaguchi, M., Kawamoto, T., Kelley, K.A., Koornneef, J.M., Kurz, M.D., Laubier, M., Layne, G.D., Lerner, A., Lin, K. Y., Liu, P.P., Lorenzo-Merino, A., Luciani, N., Magalhães, N., Marschall, H.R., Michael, P.J., Monteleone, B.D., Moore, L.R., Moussallam, Y., Muth, M., Myers, M.L., Narváez, D.F., Navon, O., Newcombe, M.E., Nichols, A.R.L., Nielsen, R.L., Pamukcu, A., Plank, T., Rasmussen, D.J., Roberge, J., Schiavi, F., Schwartz, D., Shimizu, K., Shimizu, N., Thomas, J.B., Thompson, G.T., Tucker, J.M., Ustunisik, G., Waelkens, C., Zhang, Y., Zhou, T., 2021. Silicate melt inclusions in the new millennium: a review of recommended practices for preparation, analysis, and data presentation. Chem. Geol. 570 https://doi.org/10.1016/j.chemgeo.2021.120145.
Rytuba, J.J., McKee, E.H., Cox, D.P., 1993. Geochronology and Geochemistry of the Ladolam Gold Deposit, Lihir Island, and Gold Deposits and Volcanoes of Tabar and Tatau, Papua New Guinea. (U.S. Geol. Surv. 119–126).
Schuth, S., Münker, C., König, S., Qopoto, C., Basi, S., Garbe-Schönberg, D., Ballhaus, C., 2009. Petrogenesis of lavas along the Solomon Island Arc, SW Pacific: Coupling of compositional variations and subduction zone geometry. J. Petrol. 50, 781–811. https://doi.org/10.1093/petrology/egp019.
Schwindinger, K.R., 1999. Particle dynamics and aggregation of crystals in a magma chamber with application to Kilauea Iki olivines. J. Volcanol. Geotherm. Res. 88, 209–238. https://doi.org/10.1016/S0377-0273(99)00009-8.
Scoates, J.S., 2000. The plagioclase-magma density paradox re-examined and the crystallization of Proterozoic anorthosites. J. Petrol. 41, 627–649. https://doi.org/10.1093/petrology/41.5.627.
Shaw, D.M., 1970. Trace element fractionation during anatexis. Geochim. Cosmochim. Acta 34, 237–243. https://doi.org/10.1016/0016-7037(70)90009-8.
Smith, D.J., Naden, J., Jenkin, G.R.T., Keith, M., 2017. Hydrothermal alteration and fluid pH in alkaline-hosted epithermal systems. Ore Geol. Rev. 89, 772–779. https://doi.org/10.1016/j.oregeorev.2017.06.028.
Soustelle, V., Tommasi, A., Demouchy, S., Franz, L., 2013. Melt-rock interactions, deformation, hydration and seismic properties in the sub-arc lithospheric mantle inferred from xenoliths from seamounts near Lihir, Papua New Guinea. Tectonophysics 608, 330–345. https://doi.org/10.1016/j.tecto.2013.09.024.
Stracke, A., Hegner, E., 1998. Rifting-related volcanism in an oceanic post-collisional setting: the Tabar-Lihir-Tanga-Feni (TLTF) island chain, Papua New Guinea. Lithos 45, 545–560. https://doi.org/10.1016/S0024-4937(98)00049-8.
Streck, M.J., Dungan, M.A., Malavassi, E., Reagan, M.K., Bussy, F., 2002. The role of basalt replenishment in the generation of basaltic andesites of the ongoing activity at Arenal volcano, Costa Rica: evidence from clinopyroxene and spinel. Bull. Volcanol. 64, 316–327. https://doi.org/10.1007/s00445-002-0209-2.
Taylor, B., 1979. Bismarck Sea: Evolution of a back-arc basin. Geology 7, 171–174. https://doi.org/10.1130/0091-7613(1979)7<171:BSEOAB>2.0.CO;2.
Taylor, B., 2006. The single largest oceanic plateau: Ontong Java-Manihiki-Hikurangi. Earth Planet. Sci. Lett. 241, 372–380. https://doi.org/10.1016/j.epsl.2005.11.049.
Ubide, T., Kamber, B.S., 2018. Volcanic crystals as time capsules of eruption history. Nat. Commun. 9, 1–12. https://doi.org/10.1038/s41467-017-02274-w.
Vance, J.A., 1969. On synneusis. Contrib. To Mineral. Petrol. 24, 7–29. https://doi.org/10.1007/BF00398750.
Wallace, D.A., Johnson, R.W., Chappell, B.W., Arculus, R.J., Perfit, M.R., Crick, I.H., 1983. Cainozoic Volcanism of the Tabar, Lihir, Tanga, and Feni Islands, Papua New Guinea: Geology, Whole-Rock Analyses, and Rock-Forming Mineral Compositions. Report, Bur. Miner. Resour. Aust, p. 243.
Wood, B.J., Trigila, R., 2001. Experimental determination of aluminous clinopyroxene-melt partition coefficients for potassic liquids, with application to the evolution of the Roman province potassic magmas. Chem. Geol. 172, 213–223. https://doi.org/10.1016/S0009-2541(00)00259-X.
Woodhead, J., Hergt, J., Sandiford, M., Johnson, W., 2010. The big crunch: Physical and chemical expressions of arc/continent collision in the Western Bismarck arc. J. Volcanol. Geotherm. Res. 190, 11–24. https://doi.org/10.1016/j.jvolgeores.2009.03.003.
Workman, R.K., Hart, S.R., 2004. Major and Trace Element Composition of the Depleted MORB Mantle (DMM). Earth Planet. Sci. Lett.
Zhu, Y.X., Wang, L.X., Ma, C.Q., Zhang, C., 2018. A flower-like glomerophyric diorite porphyry from Central China: Constraints on the unusual texture. Lithos 318–319, 1–13. https://doi.org/10.1016/j.lithos.2018.07.031.